SLAC-PUB-544
January 1969
(TH) & (EXP)

SINGLE AND DOUBLE PION PRODUCTION BY OPE AND A COMPARISON WITH EXPERIMENTAL DATA BETWEEN 1.6 AND 20 GeV/c*

by

Günter Wolf**
Stanford Linear Accelerator Center
Stanford University, Stanford, California

ABSTRACT

A detailed comparison has been made between predictions of elementary one-pion exchange (OPE) and existing experimental data. The Benecke-Dürr (BD) parametrization was used to describe the vertex functions. The BD parametrization has one free parameter, R, for each vertex. The momentum transfer (t) distributions as measured between 1.6 GeV/c and 10 GeV/c for the reactions $\bar{p}p \longrightarrow \overline{\Delta^{++}}\Delta^{++}$ ($\Delta \equiv \Delta(1236)$), $pp \longrightarrow \Delta^{++}n$, $\pi^+p \longrightarrow \Delta^{++}\rho^o$ and $\pi^-p \longrightarrow n\rho^o$ were used to fit the parameters $R_{\Delta N\pi}$, $R_{NN\pi}$ and $R_{\rho\pi\pi}$ which describe the $NN\pi$, $\Delta N\pi$ and $\rho\pi\pi$ vertices. With the 3-parameter fit an excellent description of the data is achieved for $|t| < 1$ GeV^2

(Sub. to Phys. Rev.)

---

*Work supported by the U. S. Atomic Energy Commission and the Bundesministerium für Wissenschaftliche Forschung, Germany.

**On leave of absence from the Deutsches Elektronen Synchrotron (DESY).

at all energies, a result which independent of any model demonstrates that the energy dependence of these reactions is that of elementary one-pion exchange. From the R parameters values for various pionic rms radii were deduced:

$$\langle r^2_{NN\pi}\rangle^{1/2} = (1.06 \pm 0.04)\text{f}, \quad \langle r^2_{\Delta N\pi}\rangle^{1/2} = (0.86 \pm 0.02)\text{f}$$

and $\langle r^2_{\rho\pi\pi}\rangle^{1/2} = (0.65 \pm .05)$f. The $NN\pi$ and $\Delta N\pi$ values agree with results from πN and ep scattering. As a further consistency check, the BD parametrization was used to describe δ_{33}, the (3/2, 3/2) pion nucleon phase shift, in the neighborhood of the Δ. A good fit to the δ_{33} data is found with a value for $R_{\Delta N\pi}$ which agrees within 20% of that from the fit to the t distributions. The OPE predictions were calculated for the reactions $\pi^{\pm}p \rightarrow p\pi^{+}\pi^{\pm}\pi^{-}$ in absolute magnitude and compared with available experimental results on effective mass — and momentum transfer distributions at beam momenta between 2.1 GeV/c and 20 GeV/c. In general, the shape of the distributions is quite well reproduced. Bumps which are present in the $p2\pi$ mass distributions and which may be taken as evidence for the production of nucleon isobars can be understood as reflections of the OPE process. The OPE contributions are substantial at all energies; they amount to ~40% near threshold and increase to ~90% at 20 GeV/c, in contrast to the naive (?) expectation that at higher energies the exchange of particles with higher spin dominates.

I. INTRODUCTION

Since the idea of the dominance of the One-Pion Exchange (OPE) was developed a decade ago,[1] numerous OPE calculations have been carried out using different techniques to calculate off-mass shell corrections for the vertex functions involved. For some reactions, a quite successful description of the experimental data was achieved by either using a form factor approach or by applying absorption corrections.[2,3] However, in general, these models predicted much too high cross sections for processes where particles with higher spins are involved such as $\pi^- p \longrightarrow n f^o$.[4]

The failure can be traced back to the Born approximation which is used to calculate the off-shell behavior of the vertex functions. At this stage, Dürr and Pilkuhn proposed, in analogy to potential scattering, to use instead of the Born factors the complete penetration factors for the angular momentum barrier.[5] This type of off-shell correction overcomes the difficulties with particles of higher spin. Following Dürr and Pilkuhn, it was found that experimental data on the processes $\pi^+ p \longrightarrow \Delta^{++} \rho^o$ (where Δ is the 33 πN resonance with a mass of 1.236 GeV) and $\bar{p}p \longrightarrow \bar{\Delta}^{++} \Delta^{++}$ were well described by the OPE model for four-momentum transfers squared up to ~0.6 GeV^2.[6] However, at larger momentum transfers, the theoretical cross sections were still larger than those measured experimentally.

Recently, a more satisfactory modification of the vertex functions was proposed by Benecke and Dürr which retains the previous advantage but which leads to a rapid fall off of the vertex functions with high momentum transfers.[7] Their approach introduces one free parameter R for each partial wave contributing to the vertex function. The parameters R have to be determined from experimental

data. It will be shown that having fitted the parameters R_N, R_Δ and R_ρ for the $NN\pi$, $N\Delta\pi$ and $\rho\pi\pi$ vertices the OPE model gives an excellent description of the experimental differential cross sections up to $|t| = 1\ GeV^2$ measured at incoming momenta between 1.6 GeV/c and 16 GeV/c for the processes

$$\bar{p}p \longrightarrow \bar{\Delta}^{++}\Delta^{++} \tag{1}$$

$$pp \longrightarrow \Delta^{++}n \tag{2}$$

$$\pi^+ p \longrightarrow \Delta^{++}\rho^o \tag{3}$$

$$\pi^- p \longrightarrow n\rho^o \tag{4}$$

The rms radii, $\langle r^2\rangle^{1/2}$, derived for the vertices from the fitted vertex functions are consistent with ep and πp scattering: The pionic radius of the nucleon turns out to be $\langle r^2_{NN\pi}\rangle^{1/2} = (1.06 \pm 0.04)$f which is about 20% larger than the electric charge radius, but which agrees well with the rms radius for πN scattering of 1.1f obtained from an optical model analysis of πN diffraction scattering data. The result for the $\rho\pi\pi$ vertex is $\langle r^2_{\rho\pi\pi}\rangle^{1/2} = (0.65 \pm 0.05)$f. The rms radius for the $\Delta N\pi$ vertex, $\langle r^2_{\Delta N\pi}\rangle^{1/2} = (0.86 \pm 0.02)$f is within the errors the same as that found for the $\Delta N\gamma$ vertex. In case of the $\Delta N\pi$ vertex, an additional consistency check was made by fitting the (on shell) δ_{33} phase shift to the Benecke-Dürr parametrization. A good description of δ_{33}, i.e. of the energy dependence of the Δ width, is achieved for cms energies up to 1.42 GeV with $R_\Delta^{\text{on shell}} = (2.2 \pm 0.1)GeV^{-1}$, a value which agrees within 20% with $R_\Delta^{\text{off shell}} = (1.76 \pm 0.03)GeV^{-1}$ as obtained from the fit to the momentum transfer distributions.

The close agreement of the OPE curves with the data for reactions (1) - (4) leads to the following conclusions:

a) The energy behavior of the measured differential cross sections for (1) - (4) is that of elementary one pion exchange (the off-shell corrections applied depend only on the momentum transfer).

b) At small momentum transfers (several pion mass squared) the off-shell corrections approach those given by the Born approximation (which is believed to be correct near the pole). The magnitude of the cross section predicted by the OPE model for small momentum transfers is therefore essentially a consequence of the (measured) values of the $\Delta N\pi$ and $\rho\pi\pi$ decay widths. The agreement at small momentum transfers then means that there the differential cross sections for (1) - (4) are of the order expected for elementary OPE.

A third evidence in favor of one-pion exchange comes from the Δ and ρ decay distribution observed for (1) - (4): they require a dominant contribution from the exchange of a $J^P = 0^-$ object (see also remark below).

Finally a recent direct check of the OPE model has been made by Schlein and co-workers[8] in the case of the reaction $pp \longrightarrow pn\pi^+$. The experimental differential cross sections for this reaction at small momentum transfers were used to determine the π^+p elastic scattering cross section, $\sigma_{\pi^+p}(M)$, in the region of the 33 πN resonance by a Chew Low extrapolation. A comparison with the measured values of $\sigma_{\pi^+p}(M)$ was made. It was found that the result depends critically on the extrapolation function used. A remarkably good agreement was accomplished with the Dürr-Pilkuhn parametrization which at small momentum transfers is equivalent to that of Benecke and Dürr.

These evidences have been taken as a justification for the present analysis. The production mechanism for reactions (1) - (4) may, however, be much more complicated and the success of the elementary OPE model accidental. In such a case, the model still has some merit in that it allows the description of a large amount of experimental data with few free parameters. With all these precautions in mind, we assume from now on, that the dominance of elementary one-pion exchange is a good hypothesis.

Encouraged by the success for reactions (1) - (4), an attempt was made to determine the extent to which OPE explains features of the reactions:

$$\pi^+ p \longrightarrow p\pi^+\pi^+\pi^- \tag{5}$$

$$\pi^- p \longrightarrow p\pi^+\pi^-\pi^- \tag{6}$$

To this end, the R parameters for all $\pi\pi \longrightarrow \pi\pi$ and $\pi N \longrightarrow \pi N$ partial waves which enter into the calculation of the vertex functions have to be determined. This is achieved by using experimental data on the reactions $\pi^- p \longrightarrow n\pi^+\pi^-$, $\pi^- p \longrightarrow \Delta^{++}\pi^-\pi^-$ and $\pi^- p \longrightarrow p\pi^-\rho^o$. As a by-product, the T = 2 $\pi\pi$ elastic scattering cross section is obtained.

In calculating the OPE contributions to the reactions $\pi^\pm p \longrightarrow p\pi^\pm\pi^+\pi^-$, all possible OPE diagrams are evaluated but the interference terms are neglected. The comparison with the experimental data is done for the entire range of beam momenta over which these reactions have been studied, i.e., from 2 GeV/c to 20 GeV/c. The following conclusions can be drawn:

1. The OPE contributions are quite substantial: They amount to ~ 40% of the total reaction near threshold and increase to ~ 90% at 20 GeV/c! This result is quite surprising because, naively, one expects at higher energies the exchange of vector mesons and/or particles of higher spin to become the dominant processes.
2. The shape of mass distributions and of distributions of various other kinematical quantities which have been studied are rather well reproduced by the calculation. This is especially true if the contribution of one of the OPE diagrams is isolated, (which can be done by making a cut in the four-momentum transfer and/or selecting events in the Δ^{++} and/or ρ^o regions).

Similar OPE calculations, applying Ferrari-Selleri corrections, have been done earlier for reaction (5) at 4 GeV/c incident momentum.[9] Recently, Raubold[10] has investigated the OPE contributions for the reactions (5) and (6), using the Dürr-Pilkuhn parametrization and taking the interference terms between the different OPE diagrams into account. He concludes that above 4 GeV/c the OPE model gives a fair description of these reactions.

One remark is in place concerning the decay-angular distributions of, say, the isobars produced in $\bar{p}p \rightarrow \Delta^{\overline{++}} \Delta^{++}$. It is well known that deviations from isotropy are observed in the distribution of the azimuthal decay angle of the isobar, in contrast to the prediction of a pure OPE model such as the one used here. It is also known that the observed deviations in the decay distributions can be explained by the absorption model for OPE.[3f] Therefore, an adequate description of both differential cross section and decay distribution, can be expected from an OPE model which uses the Benecke-Dürr parametrization for vertex functions and takes absorptive effects due to initial state and final state interaction into account. Such a calculation has not yet been done.

II. THE OPE CROSS SECTION AND THE BENECKE-DÜRR PARAMETRIZATION

In this section the cross section formula for a typical OPE diagram is given, in the Benecke-Dürr approach. We consider the contribution of the diagram (a) in Fig. 1 to the reaction $\pi^+ p \rightarrow p\pi^+\pi^+\pi^-$. The following definitions are made:

$$\pi^+_{in},\ P_{in},\ P_{out},\ \pi^+_a,\ \pi^+_b,\ \pi^-$$

are the four-momentum vectors of the corresponding incoming and outgoing particles.

$s = (\pi^+_{in} + p_{in})^2$ — square of total cm energy.

p^* - c.m. momentum in the initial state.

$t = \left(p_{in} - (p_{out} + \pi_b^+)\right)^2$ — square of the four momentum transfer.

μ - pion mass

m_p - nucleon mass

$m^2 = (\pi_a^+ + \pi^-)^2$ — square of $\pi_a^+ \pi^-$ rest mass.

θ - angle between incoming π^+ and outgoing π_a^+ in the $\pi_a^+\pi^-$ rest frame.

q_t - momentum of the exchanged pion in the $\pi_a^+\pi^-$ rest frame.

$q_t = P(t, \mu^2, m^2)$ where

$$P\left(m_1^2, m_2^2, m_3^2\right) = \left[\frac{m_1^4 - 2m_1^2\left(m_2^2 + m_3^2\right) + \left(m_2^2 - m_3^2\right)^2}{4m_3^2}\right]^{1/2}$$

$M^2 = \left(p_{out} + \pi_b^+\right)^2$ — square of $p\pi_b^+$ rest mass.

$\circledast$ — angle between incoming and outgoing proton in $p_{out}\pi_b^+$ rest frame.

$Q_t = P(t, m_p^2, M^2)$ momentum of the exchanged pion in the $p_{out}\pi_b^+$ rest frame.

$$\frac{d\sigma_{\pi^+\pi^-}(m, \cos\theta, t)}{d\cos\theta} \quad , \quad \frac{d\sigma_{p\pi^+}(M, \cos\circledast, t)}{d\cos\circledast}$$

differential cross sections for the reactions $\pi^+\pi^- \longrightarrow \pi^+\pi^-$ and $\pi^+p \longrightarrow \pi^+p$ respectively where one of the incoming pions is virtual with a mass squared of t.

The differential cross section corresponding to the diagram a) of Fig. 1 is given by the following expression:[11]

$$\frac{d^5\sigma}{d|t|\, d\, m\, d\cos\theta\, d\, M\, d\cos\theta} =$$

$$\frac{1}{4\pi^3 p^{*2}_s}\, m^2 q_t\, \frac{d\sigma_{\pi^+\pi^-}(m, \cos\theta, t)}{d\cos\theta}\, \frac{G^2(t)}{(t-\mu^2)^2}\, *M^2 Q_t\, \frac{d\sigma_{p\pi^+}(M, \cos\circledast, t)}{d\cos\circledast} \qquad (7)$$

Here G(t) is a correction to the pion propagator. The other unknowns in Eq. (7)

are the off-shell cross sections $\frac{d\sigma_{\pi^+\pi^-}(m, \cos\theta, t)}{d\cos\theta}$ and $\frac{d\sigma_{p\pi^+}(M, \cos\circledast, t)}{d\cos\circledast}$,

which are connected to the corresponding on-shell cross sections

$\frac{d\sigma_{\pi^+\pi^-}(m, \cos\theta)}{d\cos\theta}$ and $\frac{d\sigma_{p\pi^+}(m, \cos\circledast)}{d\cos\circledast}$ for elastic $\pi^+\pi^-$ and $p\pi^+$ scattering.

If we now assume that the scattering at both vertices, takes place in states with definite angular momentum ℓ and L and definite parity, we can replace $\sigma_{\pi^+\pi^-}(m, t)$ and $\sigma_{p\pi^+}(M, t)$ by their partial cross sections $\sigma^{\ell}_{\pi^+\pi^-}(m, t)$ and $\sigma^{L}_{p\pi^+}(M, t)$. (This is, of course, true also for the differential cross sections.)

In the Born approximation, the off-shell cross sections are related to the on-shell cross sections by[11]

$$q_t\, \sigma^{\ell}_{\pi^+\pi^-}(m, t) = \left(\frac{q_t}{q}\right)^{2\ell} q\sigma_{\pi^+\pi^-}(m) \tag{8}$$

and

$$Q_t \sigma^{L}_{p\pi^+}(M, t) = \left[\frac{K^t_{\pm}}{K_{\pm}} \frac{Q_t^{J-1/2}}{Q^{J-1/2}}\right]^2 Q\sigma^{L}_{p\pi^+}(m) \tag{9}$$

where J is the total spin of the πN state, q and Q are the $\pi\pi$ and πN cms momenta:

$$q = P(\mu^2, \mu^2, m^2)$$

$$Q = P(\mu^2, m_p^2, M^2)$$

and

$$K^t_{\pm} = \sqrt{(M \pm m_p)^2 - t}$$

$$K_{\pm} = \sqrt{(M \pm m_p)^2 - \mu^2}$$

and the +(-) sign applies for positive (negative) intrinsic parity of the πN state.

The following form of Eq. (9) is better suited for our purpose:

For $L = J - 1/2$

$$Q_t \sigma^{L}_{p\pi^+}(M, t) = \frac{(M \pm m_p)^2 - t}{(M \pm m_p)^2 - \mu^2} \left[\frac{Q_t}{Q}\right]^{2L} Q\sigma^{L}_{p\pi^+}(M) \tag{9a}$$

and for $L = J + 1/2$:

$$Q_t \, \sigma^{L}_{p\pi^+}(M, t) = \frac{(M \mp m_p)^2 - \mu^2}{(M \mp m_p)^2 - t} \left[\frac{Q_t}{Q}\right]^{2L} Q\sigma^{L}_{p\pi^+}(M) \qquad (9b)$$

In both cases the upper (lower) sign applies for positive (negative) intrinsic parity of the πN state. As one can see from the definition of q_t and Q_t, the off-shell cross sections in the Born approximation behave like $t^{2\ell}$ and $t^{2L \pm 1}$ for large $|t|$, and, therefore, the OPE cross section may diverge for large $|t|$. This unpleasant behavior is the cause of difficulties with the OPE model when reactions involving particles with higher spin were considered.

A more appealing behavior of the off-shell cross sections is suggested by Benecke and Dürr. For convenience, some of the arguments given in their paper are repeated here. In essence, Benecke and Dürr assume that the elastic scattering of particles a and b via

$$a + b \longrightarrow a' + b'$$

can be described by the exchange of a scalar particle x with mass m_x (see Fig. 2). Then going off-mass shell with one of the particles, say particle a, the relation between the off-shell and the on-shell scattering amplitude as a function of the off-shell mass of a is obtained. As a result, the factors $\left(\frac{q_t}{q}\right)^{2\ell}$ and $\left(\frac{Q_t}{Q}\right)^{2L}$ which appear in Eqs. (8), (9a) and (9b) are replaced by the functions $\frac{u_\ell(q_t R)}{u_\ell(qR)}$ and $\frac{u_L(Q_t R)}{u_L(QR)}$:

$$q_t \, \sigma^{\ell}_{\pi^+\pi^-}(m, t) = \frac{u_\ell(q_t R)}{u_\ell(qR)} \, q\sigma^{\ell}_{\pi^+\pi^-}(m) \qquad (10)$$

For $L = J - 1/2$:

$$Q_t \sigma^{L}_{p\pi^+}(M, t) = \frac{(M \pm m_p)^2 - t}{(M \pm m_p)^2 - \mu^2} \, \frac{u_L(Q_t R)}{u_L(QR)} \, Q\sigma^{L}_{p\pi^+}(M) \qquad (11a)$$

For $L = J + 1/2$:

$$Q_t \sigma^L_{p\pi^+}(M, t) = \frac{(M \mp m_p)^2 - \mu^2}{(M \mp m_p)^2 - t} \frac{u_L(Q_t R)}{u_L(QR)} Q\sigma^L_{p\pi^+}(M) \tag{11b}$$

As before, the upper (lower) sign applies for positive (negative) parity of the πN state.

In the above expressions $\frac{1}{m_x}$ has been put equal to R, and $u_\ell(x)$ is defined by

$$u_\ell(x) = \frac{1}{2x^2} Q_\ell \left(1 + \frac{1}{2x^2}\right) \tag{12}$$

where $Q_\ell(z)$ are the Legendre Functions of the second kind. Speical cases of the functions $u_\ell(x)$ are

$$u_0(x) = \frac{1}{4x^2} \ln (4x^2 + 1)$$

$$u_1(x) = \frac{1}{2x^2} \left\{ \frac{2x^2 + 1}{4x^2} \ln (4x^2 + 1) - 1 \right\} \tag{13}$$

The functions $u_\ell(x)$ have the following general properties:

$$u_\ell(x) \sim x^{2\ell} \quad \text{for } x \ll 1 \tag{14a}$$

$$u_\ell(x) \sim \frac{1}{x^2} \ln(4x^2) \quad \text{for } x \gg 1 \tag{14b}$$

Hence, for small value of $|t|$ the off-shell cross sections have the behavior given by the Born approximation which gives the proper behavior near threshold. For large $|t|$ values, they behave like $\frac{1}{t^2}$ and $\frac{1}{t}$, $\frac{1}{t^3}$ respectively, in contrast to the Born result. The mechanism responsible for the vertex corrections will, in general, be more complicated than that described by the diagram of Fig. 2. Using the BD parametrization means that its effect will be approximated by the exchange diagram of Fig. 2 with an effective mass 1/R.

III. FIT OF G(t) AND THE R PARAMETERS

In order to evaluate the OPE cross section in the Benecke-Dürr parametrization (BD), we have to know the function G(t) and the parameters R. It is assumed that there is one parameter R for each partial wave contributing to the off-shell scattering cross sections. The function G(t) and the R parameters will be determined by fitting the OPE cross section to the differential cross sections, $d\sigma/dt$, measured experimentally. For this purpose the favorable reactions are quasi-two body reactions where one partial wave (at each vertex) dominates the off-shell cross sections. The analyses, which have been done using form factor and absorption models, indicate that the processes (1) - (4) are likely to be dominated by OPE.

The relevant OPE diagrams are shown in Fig. 3. The corresponding OPE cross sections are conveniently expressed in terms of the following quantities:

$$\left|T_{\Delta N\pi}(M, t)\right|^2 \equiv M^2 \frac{(M + m_p)^2 - t}{(M + m_p)^2 - \mu^2} \frac{u_1(Q_t R_\Delta)}{u_1(Q R_\Delta)} Q\sigma_{p\pi^+}(M) \qquad (15)$$

$$\left|T_{\rho\pi\pi}(m, t)\right|^2 \equiv m^2 \frac{u_1(q_t R_\rho)}{u_1(q R_\rho)} q\, \sigma_{\pi^+\pi^-}(m) \qquad (16)$$

$$\left|T_{NN\pi}(t)\right|^2 \equiv (-t) \frac{1 + R_N^2 q_N^2}{1 + R_N^2 q_{Nt}^2} \pi^2 g^2 \qquad (17)$$

where $q_N = P(\mu^2, m_p^2, m_p^2)$, $q_{Nt} = P(t, m_p^2, m_p^2)$ and g^2 is the $NN\pi$ coupling constant with $g^2 = 14.6$ for π^0 and $g^2 = 29.2$ for $\pi^\pm$. R_Δ, R_ρ and R_N are the R parameters for the $\Delta N\pi$, $\rho\pi\pi$ and $NN\pi$ vertices. For the $NN\pi$ vertex, the off-shell behavior is calculated a la Dürr-Pilkuhn[5] since the BD parametrization leads to complex expressions for bound state scattering.

The OPE cross sections are then given for $\bar{p}p \longrightarrow \bar{\Delta}^{++}\Delta^{++}$ by:

$$\frac{d^3\sigma}{d|t|dmdM} = \frac{1}{4\pi^3 p^{*2}_s} \left|T_{\Delta N\pi}(m, t)\right|^2 \frac{G^2(t)}{(t-\mu^2)^2} \left|T_{\Delta N\pi}(M, t)\right|^2 \quad (18)$$

for $pp \longrightarrow \Delta^{++} n$ by:[12]

$$\frac{d^2\sigma}{d|t|dm} = \frac{1}{4\pi^3 p^{*2}_s} \left|T_{\Delta N\pi}(m, t)\right|^2 \frac{G^2(t)}{(t-\mu^2)^2} \left|T_{NN\pi}(t)\right|^2 \quad (19)$$

for $\pi^+ p \longrightarrow \Delta^{++}\rho^o$ by:

$$\frac{d^3\sigma}{d|t|dmdM} = \frac{1}{4\pi^3 p^{*2}_s} \left|T_{\rho\pi\pi}(m, t)\right|^2 \frac{G^2(t)}{(t-\mu^2)^2} \left|T_{\Delta N\pi}(M, t)\right|^2 \quad (20)$$

for $\pi^- p \longrightarrow n\rho^o$ by:

$$\frac{d^2\sigma}{d|t|dm} = \frac{1}{4\pi^3 p^{*2}_s} \left|T_{\rho\pi\pi}(m, t)\right|^2 \frac{G^2(t)}{(t-\mu^2)^2} \left|T_{NN\pi}(t)\right|^2 \quad (21)$$

The differential cross sections, $d\sigma/d|t|$, for the processes (1) - (4) are obtained experimentally by considering all events in certain Δ^{++} and ρ^o mass intervals which typically are 200 MeV wide. The OPE cross sections will be integrated over exactly the same Δ^{++} and ρ^o mass regions. In this integration partial waves other than the p waves from Δ^{++} and ρ^o are contributing. Their effect on the off-shell corrections is supposed to be negligible for the Δ^{++} region. In the case of the ρ^o region, there are T = 0, 2 s wave contributions to $\sigma_{\pi^+\pi^-}(m)$ which according to $\pi\pi$ phase shift analyses, amount to 10 - 20%.[13] For these s wave contributions, a value of R = 0.01 GeV^{-1} was used in calculating the off-shell corrections. A description of how the off-shell corrections were made in the presence of several partial waves is given in the appendix. The elastic $\pi^+\pi^-$ and $\pi^+ p$ cross sections used in the calculations are shown in the appendix (Figs. 26a, c).

The experimental data[14-17] on $d\sigma/d|t|$ for the processes (1) - (4) are shown in Figs. 4 to 7 for different beam momenta. In a least squares fit simultaneously

done to all these cross section values (except those shown in Fig. 6e), the function G(t) and the parameters R_Δ, R_N and R_ρ were determined. The following ansatz has been made

$$G(t) = \frac{c - u^2}{c - t} \tag{22}$$

In a first fit, a value of 140 GeV^2 was obtained for the parameter c in (Eq. (22). Therefore, we put G(t) = 1 and the fit was repeated. The resulting values for R_N, R_Δ and R_ρ are given in Table I. The χ^2 of the fit was 161 with 98 degrees of freedom. The errors of the R parameters have consequently been increased by a factor of $\sqrt{\frac{161}{98}}$. The OPE cross sections for the processes (1) to (4) as resulting from the fit are shown by the curves in Figs. 4-7. They follow closely the experimental points for all four processes at all beam momenta. (The experimental data for $\pi^+ p \rightarrow \Delta^{++} \rho^o$ at 16 GeV/c (Fig. 6e) were not used for the fit. In this case, therefore, the OPE curve is a prediction.)

IV. DISCUSSION OF THE VERTEX FORM FACTORS

In this section we want to compare the vertex functions as obtained from the above fits with the information on these quantities from various other sources, e.g., ep and πN scattering. In doing this one has to keep in mind that the vertex functions have been determined from data at $|t| \lesssim 1$ GeV^2 and therefore they may not be applicable at larger momentum transfers. In fact the calculated OPE cross sections are larger by a few percent than those measured experimentally when integrated over all t values allowed by kinematics, implying that, in the absence of destructive interference with other processes, the vertex functions fall off more rapidly at momentum transfers $|t| > 1$ GeV^2 than those given by the BD parametrization.

1. It is common to define the form factor $F_{abe}(t)$ associated with the vertex abe as the ratio of the actual vertex function $V_{abe}(t)$ to the vertex function $V^{B}_{abe}(t)$ given in the Born approximation:

$$F_{abe}(t) = \frac{V_{abe}(t)}{V^{B}_{abe}(t)} \tag{23}$$

This leads to

$$F_{NN\pi}(t) = \left[\frac{1 + R_N^2 q_N^2}{1 + R_N^2 q_{Nt}^2}\right]^{1/2} \tag{23a}$$

$$F_{\Delta N\pi}(t) = \frac{Q}{Q_t}\left(\frac{u_1(Q_t R_\Delta)}{u_1(Q R_\Delta)}\right)^{1/2} \tag{23b}$$

$$F_{\rho\pi\pi}(t) = \frac{q}{q_t}\left(\frac{u_1(q_t R_\rho)}{u_1(q R_\rho)}\right)^{1/2} \tag{23c}$$

or in general (except for bound state scattering) to

$$F_{ab\pi}(t) = \left(\frac{q_a}{q_{at}}\right)^{\ell}\left(\frac{u_\ell(q_{at} R_{ab\pi})}{u_\ell(q_a R_{ab\pi})}\right)^{1/2}$$

with

$$q_a = P\left(\mu^2,\ m_b^2,\ m_a^2\right)$$
$$q_{at} = P\left(t,\ m_b^2,\ m_a^2\right)$$

where m_a, m_b are the masses of the particles a, b and $m_a > \mu + m_b$.

Interpreting F(t) as the Fourier transformation of a spherically symmetrical density distribution the rms radius $\langle r^2 \rangle^{1/2}$ can be calculated from[18]

$$\langle r^2 \rangle = 6\frac{dF}{dt'} \text{ evaluated at } t' = 0 \tag{24}$$

where $t' = t - t_{pole} = t - \mu^2$.

The rms radii obtained from Eq. (24) for the various vertices are given in Table I. Their values range from 0.6 to 1.1 fermi.

The pionic radius of the nucleon, $\langle r^2_{NN\pi}\rangle^{1/2} = (1.06 \pm .04)$f, is larger by about 20% than the electric charge radius of the proton, $\langle r^2_p\rangle = (0.83 \pm 0.02)$f,[19] but is rather close to the rms radius for πN interaction, $\langle r^2_{N\pi}\rangle^{1/2} = 1.1$f, as deduced from elastic πN scattering via the relation $\langle r^2_{N\pi}\rangle = 4A$. Here A is the exponential slope of the differential cross section for πN elastic scattering. The rms radius for the $\Delta N\pi$ vertex, $\langle r^2_{\Delta N\pi}\rangle^{1/2} = (0.86 \pm 0.02)$f, agrees quite well with the same quantity for the $\Delta N\gamma$ vertex: $\langle r^2_{\Delta N\gamma}\rangle^{1/2} \simeq 0.84$f. The latter value is obtained from the M1 transition form factor for the $\Delta N\gamma$ vertex as measured in inelastic ep scattering.[20]

2. In Table I the rms radii for various other vertices are also given. The fits of the corresponding R parameters are discussed in Section VI. One notices that the rms radii for the baryonic vertices are of the order of 0.8 - 0.9f and for mesonic vertices 0.6 - 0.7f, although the values of the R parameters may differ by as much as a factor of 2, due to the different masses and angular momenta involved. Therefore, a good guess for the value of R and hence for the form factor can be obtained by using Eq. (24) and choosing a proper $\langle r^2\rangle^{1/2}$ value, e.g., 0.85f for baryonic vertices and 0.65f for pionic vertices.

3. Off-shell corrections for resonance scattering and the deviation of on-shell scattering from a simple Breit-Wigner formula are intimately connected. Both are a consequence of the angular momentum barrier. According to Benecke and Dürr, the same R value which governs the off-shell behavior determines the energy dependence of the resonance width. The appropriate place to test this idea is the 33 πN resonance for which very precise phase shift data are available.[21] The dependence of δ_{33}, the 33 phase shift, on the πN rest mass M is expressed

in terms of the 33 resonance mass M_0, width Γ_0 and R_Δ by:

$$\tan \delta_{33}(M) = \frac{M_0 \Gamma(M)}{M_0^2 - M^2} \tag{25}$$

with

$$\Gamma(M) = \Gamma_0 \frac{M_0 Q}{M Q_0} \frac{u_1(R_\Delta Q)}{u_1(R_\Delta Q_0)} \tag{25a}$$

where Q_0, Q are the cm momenta for πN masses of M_0 and M respectively. Figure 8 shows δ_{33} as a function of M. Equations (25), (25a) were fitted to these values for M up to 1.42 GeV and the following parameter values were obtained:

$$M_0 = (1.233 \pm 0.001) \text{ GeV}$$
$$\Gamma_0 = (0.114 \pm 0.001) \text{ GeV}$$
$$R_\Delta = (2.2 \pm 0.1) \text{ GeV}^{-1}$$

The experimental values on δ_{33} are quite well described by the fit (see curve in Fig. 8). The important result is that the values obtained for R_Δ from off-shell scattering and from the analysis of δ_{33} agree with each other within ~20%.

V. THE PION-REGGE TRAJECTORY

The experimental measurements on $d\sigma/d|t|$ for the process (3) exhibit a striking shrinkage of the width of the forward peak with increasing beam momentum (see Fig. 6). At first glance, this may be taken as clear evidence for a Regge behavior of the pion, assuming that the process (3) is completely dominated by OPE. The OPE calculations, however, which were done for an elementary pion do show the same effect (see curves in Fig 6.). As was explained in a previous note,[6] the apparent shrinkage in the OPE model is mainly due to the large Δ^{++} and ρ^0 mass intervals over which the data have been taken.

One may ask whether the data, in addition to these kinematical effects possess any genuine shrinkage. In order to study this question, the experimental data for the reactions (1) - (4) were fitted to the following equations:

$$\frac{d\sigma_i^{Regge}}{dt} = \frac{d\sigma_i^{OPE}}{dt}\, d_i(t)\, s^{2\,\alpha(t)} \tag{26}$$

where the index i refers to the reactions (1) - (4), $\frac{d\sigma_i^{Regge}}{dt}$ are the reggeized cross sections, $\frac{d\sigma_i^{OPE}}{dt}$ are the OPE cross sections given by the Eqs. (18) - (21), $d_i(t)$ are arbitrary functions of t and $\alpha(t)$ is the effective trajectory. A factor $\frac{1}{p^{*2}_{sp}} \simeq s^{-2}$ is contained in $\frac{d\sigma_i^{OPE}}{dt}$. The factor $\frac{d\sigma_i^{OPE}}{dt}$ takes care of the proper integration of the theoretical cross sections over the mass regions.

The values obtained from the fit for $d_i(t)$ and $\alpha(t)$ are summarized in Table II. Figure 9 shows $\alpha(t)$ as a function of t. Also given in Table II are the results of a fit where the expression $d_i(t)\, s^{2\,\alpha(t)}$ was replaced by

$$d_i(t)\, s^{2\,\alpha(t)} = d_i^* \left(\frac{s}{s_0^i}\right)^{2\alpha'(0)\,(t\,-\,\mu^2)} \tag{26a}$$

where d_i and s_0^i are constants, and $\alpha'(0) \equiv \left.\frac{d\alpha}{dt}\right|_{t=0}$. The fit yields $\alpha'(0) = -(0.051 \pm 0.062)\ \mathrm{GeV}^{-2}$. The net result is that the effective trajectory is zero within the errors for $-0.6\ \mathrm{GeV}^2 < t < 0$.

VI. DETERMINATION OF FURTHER R PARAMETERS OF THE $\pi\pi$ AND πN SYSTEMS

Knowing the values of R_N, R_Δ and R_ρ, we can go on to determine the R parameters of other partial waves of the $\pi\pi$ and πN systems.

a) For instance, the experimental data on

$$\pi^- p \longrightarrow n f^o \tag{27}$$

agree with the assumption that this process is dominated by OPE. The unknowns in the OPE cross section for (27) are the elastic $\pi^+\pi^-$ cross section $\sigma_{\pi^+\pi^-}(m)$ in

the f^o region and R_f, the R parameter for the $f\pi\pi$ vertex. They were determined by fitting the OPE cross sections to the experimental cross sections $d\sigma/d|t|$ for (27) as measured at 4 GeV/c[22a] and 8 GeV/c (Fig. 10a and b).[17c] For $\sigma_{\pi^+\pi^-}(m)$ a Breit-Wigner formula centered around the f^o was used. The value obtained for R_f is

$$R_f = (3.23 \pm 1.46)\ \text{GeV}^{-1}$$

The resulting $\pi^+\pi^-$ cross section is contained in Fig. 26c. The value of $\sigma_{\pi^+\pi^-}(m) = (26 \pm 2)$ mb at the f^o mass (1.26 GeV) may be compared with the unitary limit for a T = 0, d wave contribution to $\sigma_{\pi^+\pi^-}(m)$ which is $\frac{80}{9}\pi\lambda^2 = 28.5$ mb at m = 1.26 GeV. The experimental points for $d\sigma/d|t|$ of the process (27) are well described by the fit (see the curves in Figs. 10a, b).

b) There is experimental information available[17c] (Fig. 10c) on the process

$$\pi^- p \rightarrow n g^o \qquad (28)$$

where g^o is a $\pi\pi$ resonance with mass $m_g^o = 1.66$ GeV, $T^G = 1^+$ and $J^P = 3^-(?)$. This process presumably proceeds also via OPE and therefore an analogous fit can be made to obtain $\sigma_{\pi^+\pi^-}(m)$ in the g region, and R_g. The cross section $\sigma_{\pi^+\pi^-}(m)$ in the g region as determined by the fit is given in Fig. 26c. The statistical accuracy of $\sigma_{\pi^+\pi^-}(m)$ when averaged over the g region is ± 10%. The value of $\sigma_{\pi^+\pi^-}(m)$ at $m = m_g$ of 7.5 mb is much smaller than the unitary limit for a T = 1 f wave of $28\pi\lambda^2 = 51$ mb, indicating a high inelasticity for this partial wave. This conclusion is supported by the experimental observation of a sizeable 4π decay mode for the g meson.[23] The determination of R_g is rather poor. This is due to the small number of g^o events so far observed experimentally, and to the fact that with higher $\pi\pi$ mass, the difference between on-shell momentum (q) and off-shell momentum (q_t) becomes smaller for the same t value and therefore, $d\sigma/d|t|$ is less sensitive to the value of the parameter R. With $R_g = 4.5\ \text{GeV}^{-1}$

a good description of the experimental $d\sigma/d|t|$ values is obtained. (see curve in Fig. 10c). It should be pointed out that OPE calculations using a form factor or absorption corrections fail to fit the t dependence of the cross sections for the processes (27) and (28), because of the relatively high f and g spins.[4] On the other hand, the Benecke-Dürr parametrization leads to a good fit with reasonable values for the parameter R.

c) The experimental data on the reaction

$$\pi^+ p \longrightarrow n\pi^+\pi^+ \tag{29}$$

and on the process

$$\pi^- p \longrightarrow \Delta^{++}\pi^-\pi^- \tag{30}$$

can be used to determine the $T = 2\pi\pi$ cross section, $\sigma_{\pi^\pm\pi^\pm}(m)$, and the R parameters for the different partial waves contributing. Previous OPE analyses[13a, 16e, 24, 25] of the experimental data for (29) and (30) have shown that consistent values for $\sigma_{\pi^\pm\pi^\pm}(m)$ are obtained from both reactions and for different beam momenta. The relative contributions of the $\ell = 0, 2, 4$ partial waves to $\sigma_{\pi^\pm\pi^\pm}(m)$ have been taken from a $\pi\pi$ phase shift analysis.[13a] (The exact treatment of the off-shell cross section in the presence of several partial waves, is described in the appendix.) The experimental cross sections for reaction (29) as measured at 4 GeV/c[16e] and for reaction (30) as measured at 11 GeV/c[26] and 16 GeV/c[16f] were then fitted to the corresponding OPE cross section formulae in order to find $\sigma_{\pi^\pm\pi^\pm}(m)$, and the parameters $R_{T\ell}$:R_{20}, R_{22}, R_{24}. Only experimental data at small momentum transfers $|t| \lesssim 0.5$ GeV^2, were used for the fit.

The differential cross sections $d\sigma/d|t|$ for the process (30) as measured at 11 GeV/c and 16 GeV/c are shown in Figs. 11, 12 for different $\pi^-\pi^-$ mass intervals together with the fitted OPE cross sections. Figure 13 shows the

outcome of the fit for $\sigma_{\pi^\pm\pi^\pm}(m)$. The cross section values obtained from two different reactions and at different beam momenta agree within the errors with each other. Below m = 0.5 GeV the data are statistically insignificant and do not allow to deduce $\sigma_{\pi^\pm\pi^\pm}(m)$ to better than a factor of 2 - 4. At m = 0.5 GeV $\sigma_{\pi^\pm\pi^\pm}(m)$ is of the order of 20 ± 5 mb and drops then to a value of 5 ± 2 mb at m = 1.5 GeV. About the same values for $\sigma_{\pi^\pm\pi^\pm}(m)$ were obtained earlier[13a] in a form factor analysis and recently in a study[26] very similar to that one described here which used the Dürr-Pilkuhn parametrization for the off-shell corrections. The fit yielded the following R values:

$$R_{20} = 0.0 \pm 0.01 \text{ GeV}^{-1}$$

$$R_{22} = 3.59 \pm 1.19 \text{ GeV}^{-1}$$

$$R_{24} = 4.5 \text{ GeV}^{-1}$$

The value of R_{24} is not well established for the same reasons mentioned above in the case of R_g. The small value of R_{20} indicates that the off-shell corrections for T = 2 s-wave $\pi\pi$ scattering are negligible. This result was expected since in the Benecke-Dürr model the off-shell corrections are mainly an effect of the angular momentum barrier. The value of R_{22} is approximately the same as that of R_f ($\equiv R_{02}$).

d) The main contributions to the π^+p elastic scattering below 2 GeV come from the P33 and F37 partial waves. The parameter R_{P33} has been determined above ($R_{P33} \equiv R_\Delta$). The value of R_{F37} can, in principle, be obtained from a fit to data on $pp \rightarrow p\pi^+n$ with $M_{p\pi^+}$ being in the region of the F37 resonance mass (M_{F37} = 1.95 GeV). Since M_{F37} is large, the momentum transfer distribution is not very sensitive to the value of R_{F37}. A value of 4.5 GeV^{-1} was chosen for R_{F37}. The experimental data[15b] are compatible with this value.

e) An attempt was made to determine the R parameters of the T = 1/2 πN partial waves from an OPE analysis of measurements at 11 GeV/c[27] and 16 GeV/c[16f] on the process

$$\pi^- p \longrightarrow p\pi^- \rho^0 \tag{31}$$

The OPE diagram for (31) is that of Fig. 1d with π^+ and π_a^- being in the ρ^0 mass region. Only data at small four momentum transfers between incoming π^- and outoging ρ^0 were considered. In spite of that restriction, there is a substantial amount ($\sim$ 30%) of background which is produced by the OPE diagram of Fig. 1f. Another complication comes from the fact that apart from P33 there are at least six more partial waves with significant contributions to π^-p scattering below 2 GeV, i.e., S11, P11, D13, D15, F15 and F17.[21] Because of these reasons and because of the limited statistical accuracy of the experimental data, only rough estimates of the corresponding R parameters were obtained:

$$R_{P11} = 0.34 \text{ GeV}^{-1} \quad R_{D15} = 5.5 \text{ GeV}^{-1} \quad R_{S11} = 0.03 \text{ GeV}^{-1}$$

The values of R_{D13}, R_{F15} and R_{F17} have been chosen to be 4.5 GeV^{-1}.*

VII. COMPARISON OF THE REACTIONS $\pi^{\pm}p \rightarrow p\pi^{\pm}\pi^+\pi^-$ WITH THE OPE PREDICTIONS

For the comparison of the OPE predictions with the experimental data on the reactions:

$$\pi^+ p \longrightarrow p\pi^+\pi^+\pi^- \tag{5}$$

$$\pi^- p \longrightarrow p\pi^+\pi^-\pi^- \tag{6}$$

a Monte Carlo program (OPEM) was written.[28] The program constructs events of the type (5) or (6) which then are weighted according to the OPE cross section.

*The treatment of the relative contributions of the different partial waves to the off-shell corrections for the π^-p system is discussed in the appendix.

With this method the theoretical prediction for any experimental distribution of the reactions (5), (6) can be calculated since it is also possible to compute quantities for systems involving particles from different vertices (for instance, in the case of the $p\pi^+$ distribution for reaction (5) both $p\pi^+$ masses were calculated for each Monte Carlo event).

This type of Monte Carlo calculations can be very computer-time consuming, especially at high beam momenta where the kinematical allowed range of four momentum transfers is large and where, therefore, the majority of Monte Carlo events may have an extremely small weight, depending on the method used for constructing these events. The ideal method of constructing Monte Carlo events is one which leads to the same weight for each event — as nature does. A procedure which within a factor of 2 - 4 achieves this goal and which was applied in the calculation, is described in the appendix. In evaluating the OPE cross sections, the vertex functions were put equal to zero for momentum transfers $|t| > 1\,GeV^2$ for reasons discussed in Section IV.

A. The reaction (5) $\pi^+p \longrightarrow p\pi^+\pi^+\pi^-$

There are three OPE diagrams (Fig. 1a - c) which contribute to reaction (5). The diagrams a and b, which give identical contributions are dominating by far the OPE cross section since the elastic $p\pi^+$ and $\pi^+\pi^-$ cross sections are on the average much larger than the elastic $p\pi^-$ and $\pi^+\pi^+$ cross sections. Therefore, as the R parameters relevant for the $p\pi^+$ and $\pi^+\pi^-$ systems have been obtained with fair accuracy, the OPE predictions for the reaction (5) are supposed to be sound, except for the negligance of terms due to the interference of the three diagrams.

The comparison of the OPE predictions with the experimental data[16e, f, 29, 30] was at beam momenta between 1.95 GeV/c and 16 GeV/c. Since

there is no free parameter left the OPE calculation gives predictions which are absolute in magnitude. The mass and momentum transfer distributions, as measured at different momenta, are shown in Figs. 14 - 17 together with the OPE curves.

The outstanding features of reaction (5) are the production of Δ^{++}, ρ^{o} and f^{o}, a substantial fraction of which is due to the formation of the two body states $\Delta^{++}\rho^{o}$ and $\Delta^{++}f^{o}$ (see Figs. 14c; 15e, f; 16b, d; 17b, d). Comparing the experimental distributions with the OPE predictions, one notices that:

1. The fraction of the OPE contribution to reaction (5) increases with increasing momentum (see also Table III), being 40% at 2 GeV/c and ~90% at 16 GeV/c.

2. The amount of Δ^{++} production is correctly predicted to within 25% over the whole momentum range. At 2 GeV/c there appears to be a discrepancy with respect to the position of the Δ^{++}: experimentally, the Δ^{++} contribution is centered at ~ 1220 MeV whereas the OPE curve peaks at ~1190 MeV.

3. The observed cross section for ρ^{o} production is larger than that predicted by OPE. The difference can readily be explained by A_2 production via

$$\pi^{+}p \longrightarrow pA_2^{+}$$

with A_2 subsequently decaying into $\rho^{o}\pi^{+}$. The cross section for this reaction is ~ 0.3 mb at 4 GeV/c[16e] and ~ 0.2 mb at 16 GeV/c.[16f] The A_2 meson, of course, cannot be produced via OPE in this reaction.

4. The agreement between theory and experiment is particularly good whenever the contribution of one of the diagrams is separated out. This is done by either requiring a small momentum transfer to one of the $\pi\pi$ or πN mass combinations or by selecting events in either the ρ^{o} or Δ^{++} band.

B. The reaction (6) $\pi^- p \rightarrow p\pi^+\pi^-\pi^-$

Three OPE diagrams can contribute to reaction (6). They are shown in Figs. 1d -f. All three diagrams are of the same strength but only for the first two diagrams (where $\pi^-\pi^-$ are produced at one vertex and $p\pi^+$ at the other) can the contributions be calculated with some confidence. The R parameters for the $\pi^- p$ system are less accurate and therefore the OPE cross section given by the third diagram are not well determined.

For the comparison with the OPE model experimental data for beam momenta between 2.1 GeV/c and 20 GeV/c were considered[31, 22, 32, 33, 16f, 34]. The Figs. 18-25 show distributions of effective masses and momentum transfers at various momenta. The $p\pi^+$ and $\pi^+\pi^-$ mass distributions exhibit strong Δ^{++} and ρ^0 signals respectively. In addition, production of Δ^0 and of nucleon isobars around 1500 MeV and 1700 MeV is present in the $p\pi^-$ mass distributions. Again the OPE curves are predictions for shape and magnitude of the cross sections. If we take the OPE predictions at face value, conclusions very similar to those for reaction (5) can be drawn:

1. The fraction of the OPE contribution to reaction (6) increases with increasing momentum (see also Table IV), being ~ 40% at 2 GeV/c and ~ 90% at 16 GeV/c. At 20 GeV/c the OPE cross section seems to be larger than the experimental one by about ~ 5-10%.

2. The shape of the $\pi^+ p$ mass distribution in the Δ mass region and the cross section for Δ^{++} production is remarkably well reproduced for momenta above ~ 4 GeV/c.

3. The observed amount of ρ^0 production is larger than predicted by OPE. Again the difference can be explained by A_2 production via

$$\pi^- p \rightarrow p\, A_2^-$$

with A_2^- decaying into $\rho^0\pi^-$. This conclusion is supported by the $\pi^+\pi^-$ mass distribution shown in Fig. 22h for events outside the A region. There the OPE curve is in close agreement with the data.

4. The OPE model predicts the production of Δ^0, N_{1518}(D13) and N_{1688}(F15), all of which show up in the $p\pi^-$ mass distributions. The agreement with the experimental $p\pi^-$ mass distributions is quite remarkable for events which are produced at small momentum transfers and which are free from reflections from Δ^{++} production (Fig. 22f, g).

5. The $p\pi^+\pi^-$ mass distributions exhibit an accumulation of events at the low mass end and a strong peak at high masses (Figs. 21b, 22d, 23h, 24c). The high mass peak is well accounted for by the OPE model and is there a consequence of the peripheral production of the $\pi\pi$ system and of the forward peaked πN scattering angular distribution entering at the baryon vertex. The low mass bump becomes more pronounced if events in the Δ^{++} region are selected and those with a $\pi^+\pi^-$ mass combination in the ρ^0 region are excluded; a strong peak centered around $\sim$ 1550 MeV emerges (see Fig. 22e). Now, the OPE curve nearly matches this peak. Hence, the peak at 1550 MeV is — at least partly — of kinematical origin, and cannot be taken as evidence for the production of N_{1518} and/or N_{1688} and for their decays into $p\pi^+\pi^-$ unless one wants to invoke the Chew-Pignotti mechanism[35a]. The situation is reminiscent of that of the A region in the 3π mass spectrum of reactions (5) and (6).

6. In Fig. 25, some momentum transfer distributions, measured at 13 GeV/c and 20 GeV/c are compared with the OPE model. If events from the Δ^{++} region are selected which have no $\pi^+\pi^-$ combination in the ρ^0 region (i.e., isolation of the OPE diagram of Fig. 1f) the OPE predictions agree perfectly with experiment (Fig. 25a, b). If the opposite selection is made (i.e., ρ^0, no Δ^{++}), the OPE curves agree only at small momentum transfers with the data, the experimental

cross sections being larger at higher momentum transfers (Fig. 25c, d). The discrepancy can be traced back to ρ^0 mesons coming from A_2 decay (see above).

As mentioned above, the OPE contributions for reactions (5) and (6) were calculated neglecting the interference terms between the OPE diagrams. The analysis of Raubold[10] indicates these terms to give a sizeable positive contribution at medium beam momenta and a small one at higher beam momenta ($\gtrsim$ 6 GeV/c). Therefore, one expects the differences between the present OPE calculations and the experimental data for (5) and (6) at lower energies to become even smaller when these interference terms are included in the calculation.

No attempt has been made to attack the problem of the A region which is commonly referred to as the Deck effect,[35b] the reason being that the interference terms mentioned above cannot be neglected when dealing with this question.

ACKNOWLEDGEMENTS

I would like to thank the bubble chamber groups at SLAC, Harvard, Rutgers, at the Columbia University, the Genova-Hamburg-Milano-Saclay collaboration, in particular Drs. W. B. Johnson, M. Law, M. Ioffredo, Prof. Ch. Baltay and Dr. P. Von Handel for providing data prior to publication. For interesting discussions I am indebted to Drs. G. B. Chadwick, F. Gilman, Prof. D.W.G.S. Leith, Dr. A. Levy and Prof. P. Schlein. It is a pleasure to acknowledge the encouragement I experienced from Dr. G. B. Chadwick and Prof. D.W.G.S. Leith.

APPENDIX I

OFF-SHELL SCATTERING IN THE PRESENCE OF SEVERAL PARTIAL WAVES

Consider the case of $\pi^+\pi^- \to \pi^+\pi^-$ scattering with one of the incoming pions having a mass squared of t, and all other pions being on the mass shell. With the definitions of Section II:

m $\pi^+\pi^-$ rest mass,

q_t = $P(t, \mu^2, m^2)$ initial state momentum in the $\pi^+\pi^-$ frame,

q = $P(\mu^2, \mu^2, m^2)$ final state momentum in the $\pi^+\pi^-$ rest frame,

θ cm scattering angle, i.e., angle between incoming and outgoing π^+ in $\pi^+\pi^-$ rest frame.

The off-shell differential cross section for this process is given by

$$\frac{d\sigma(m, \cos\theta, t)}{d\cos\theta} = \frac{8\pi}{m^2}\frac{q}{q_t}\left|\sum_T C_T A^T(m, \cos\theta, t)\right|^2$$

$$= \frac{8\pi}{m^2}\frac{q}{q_t}\left|\frac{1}{3}A^0(m, \cos\theta, t) + \frac{1}{2}A^1(m, \cos\theta, t)\right.$$

$$\left. + \frac{1}{6}A^2(m, \cos\theta, t)\right|^2 \qquad \text{(A1)}$$

The partial wave expansion for the isospin amplitudes $A^T(m, \cos\theta, t)$ reads

$$A^T(m, \cos\theta, t) = \frac{m}{q}\sum_\ell (2\ell + 1)\, a_\ell{}^T(m, t)\, P_\ell(\cos\theta) \qquad \text{(A2)}$$

$P_\ell(\cos\theta)$ are the Legendre polynomials; following Benecke and Dürr the amplitudes $a_\ell{}^T(m, t)$ are expressed in terms of the on-shell scattering phase shifts δ_ℓ^T, the inelasticity coefficients η_ℓ^T and the parameters R_ℓ^T:

$$a_\ell^T(m, t) = \frac{1}{2i}\left[\eta_\ell^T e^{2i\delta_\ell^T} - 1\right]\left[\frac{u_\ell(q_t R_\ell^T)}{u_\ell(qR_\ell^T)}\right] \qquad \text{(A3)}$$

The functions $u_\ell(x)$ are defined in Eq. (12). If only one partial wave contributes, one obtains

$$q_t \frac{d\sigma}{dm}(m, t) = C_T^2 \frac{16\pi}{q^2} (2\ell + 1) \left| a_\ell^T(m, t) \right|^2$$

$$= C_T^2 \frac{u_\ell(q_t R_\ell^T)}{u_\ell(q R_\ell^T)} q \, \sigma^{\ell, T}(m) \qquad \text{(A4)}$$

where the meaning of the coefficient C_T can be read off from Eq. (A1); $\sigma^{\ell, T}(m)$ is the partial-wave cross section and $C_T^2 \, \sigma^{\ell, T}(m)$ is the contribution of the partial wave to the on-shell elastic scattering cross section if all other partial wave amplitudes are zero. In the OPE calculations, instead of Eqs. (A1) - (A3), the following approximation was used:

$$q_t \frac{d\sigma_{\pi^+\pi^-}(m, \cos\theta, t)}{d\cos\theta} \simeq \left(\sum_T \sum_\ell b_\ell^T \frac{u_\ell(q_t R_\ell^T)}{u_\ell(q R_\ell^T)} \right) q \sigma_{\pi^+\pi^-}(m) \frac{dW(\cos\theta)}{d\cos\theta} \qquad \text{(A5)}$$

with

$$b_\ell^T = \frac{C_T^2 \sigma^\ell_{\pi^+\pi^-}(m)}{\sum_T \sum_\ell C_T^2 \sigma^{\ell, T}_{\pi^+\pi^-}(m)}, \quad \text{i.e.,} \quad \sum_T \sum_\ell b_\ell^T = 1 \qquad \text{(A6)}$$

In Eq. (A5), $\sigma_{\pi^+\pi^-}(m)$ is the total on-shell elastic scattering cross section, $\frac{dW(\cos\theta)}{d\cos\theta}$ gives the on-shell scattering angular distribution with

$$\int_{-1}^{1} \frac{dW(\cos\theta)}{d\cos\theta} \, d\cos\theta = 1$$

The approximations made in Eq. (A5) are twofold: The off-shell corrections are weighted by the partial wave cross sections, and not according to Eq. (A3); the off-shell angular distribution is taken to be equal to the on-shell angular distribution. For $\pi^+\pi^+$ and πN scattering, formulae analogous to (A1) - (A6) apply. Eq. (A5) is exact if only one partial wave amplitude is non zero; therefore, a

good approximation of $\frac{d\sigma(m, \cos\theta, t)}{d\cos\theta}$ is obtained whenever one partial wave dominates the scattering amplitude, which is the case in the ρ^o and f^o regions for $\pi^+\pi^-$ scattering, and in the Δ region for πN scattering. In the case of $\pi^- p$ scattering, several partial waves of the same strength are present in the region from 1500 MeV to 1700 MeV cm energy. Since, however, the R parameters for the $T = \frac{1}{2}$ πN system are not well determined, it is felt that Eq. (A5) gives an adequate approximation also for this region.

APPENDIX II

$\pi\pi$ AND πN SCATTERING DATA USED AS INPUT TO THE OPE CALCULATIONS

A. πN Scattering

The cross sections for elastic π^+ - p scattering as shown in Figs. 26a, b were taken from a compilation of Foccaci and Giacomelli.[36] For the angular distributions, the experimental data of Lach[37] and of Helland et al.,[38] were used up to M = 2.1 GeV. At higher energies the angular distributions were described by an exponential form appropriate for diffraction scattering:

$$\frac{dW}{d\cos\theta} = \frac{2BQ^2}{1 - e^{-4BQ^2}} e^{-2BQ^2(1 - \cos\theta)} \qquad \text{(A7)}$$

with $Q = P(\mu^2, m_p^2, M^2)$ being the cm momentum and $B = 7.0$ GeV^{-2} and 7.7 GeV^{-2} for π^+p and π^-p scattering respectively.

The coefficients b_ℓ^T were taken from the phase shift analysis of Bareyre et al.[39]

B. $\pi\pi$ Scattering

Figures 26c, d show the $\pi^+\pi^-$ and $\pi^\pm\pi^\pm$ elastic scattering cross sections. They are based on phase shift analyses[13a, d] and on the fit results discussed in Section VI. Polynomials in $\cos\theta$ were used to describe the $\pi\pi$ angular distributions at lower energies:

$$\frac{dW}{d\cos\theta} = \sum d_n \cos^n\theta$$

The coefficients d_n are listed in Table IV. At higher energies, m > 1.4 GeV the equivalent expression to Eq. (A7) was used with $B = 5.6$ GeV^{-2} for both $\pi^+\pi^-$ and $\pi^\pm\pi^\pm$ scattering.

The values of the coefficients b_ℓ^T were estimated from phase shift analyses.[13a, d]

APPENDIX III

MONTE CARLO INTEGRATION

The Monte Carlo integration of a function f(x) over the interval $\{x_a, x_b\} = x_a < x < x_b$ is done by calculating f(x) at N points x_i, i = 1, ..., N, randomly distributed in $\{x_a, x_b\}$ and summing up:

$$\int_{x_a}^{x_b} f(x)\,dx = \lim_{N\to\infty} \sum_{i=1}^{N} f(x_i)\,\frac{x_b - x_a}{N} \tag{A8}$$

The Monte Carlo integration of the OPE cross section for say, the diagram of Fig. 1a is done in the same way. According to Eq. (7), the cross section is given by

$$\frac{d^7\sigma(t,\ m,\ \theta,\ \phi,\ M, \Theta, \Phi)}{d|t|d\ m\ d\cos\theta\ d\phi\ d\ M\ d\cos\Theta\ d\Phi}$$

$$= \frac{1}{4\pi^3 p^* s}\ m^2 q_t\ \frac{1}{2\pi}\ \frac{d\sigma_{\pi^+\pi^-}(m,\ \cos\theta,\ t)}{d\cos\theta}\ \frac{1}{(t-\mu^2)^2}$$

$$*M^2 Q_t\ \frac{1}{2\pi}\ \frac{d\sigma_{p\pi^+}(M,\ \cos\Theta,\ t)}{d\cos\Theta} \tag{A9}$$

In contrast to Eq. (7), the integration over the azimuthal angles ϕ and Φ (Treiman Yang angles) in the $\pi^+\pi^-$ and $p\pi^+$ rest systems has not yet been carried out in Eq. (A9). The Monte Carlo integration of (A9) then consists in chosing N sets y_i: t_i, m_i, θ_i, ϕ_i, M_i, Θ_i, Φ_i randomly distributed over the volume $t_a < t < t_b, \ldots, \Phi_a < \Phi < \Phi_b$ and summing the OPE weights g_i:

$$g_i = \frac{d^7\sigma(t_i,\ m_i,\ \ldots,\ \Phi_i)}{d\ t\ dm \ldots d\Phi} * \frac{(t_b - t_a)(m_b - m_a)\ldots(\phi_b - \phi_a)}{N} \tag{A10}$$

The volume $t_a < t < t_b, \ldots, \Phi_a < \Phi < \Phi_b$ contains the whole kinematically allowed region. For parameter sets y_i beyond the kinematic limit the weight

g_i is set equal to zero. From the set y_i the four momentum vectors P_J^i, J = 1, ..., 4 of the four final state particles can be constructed. Hence, we now have events defined by the vectors P_J^i and can as for real events, calculate the distribution of any quantity derived from those, the only difference being that the weights of the events are not equal to unity, but given by g_i.

Transformation of Variables:

A Monte Carlo integration of the OPE cross section in terms of the variable set y_i is not very efficient: the OPE cross section is large only a) for small values of |t|, b) when m is in the ρ^0 region and/or M in the Δ region, c) when $\cos\theta \simeq 1$, $\cos\Theta \simeq 1$ in the case of high $\pi^+\pi^-$ and $p\pi^+$ masses. The main variation of the OPE cross section comes from $\frac{1}{(t-\mu^2)^2}$, $\sigma_{\pi^+\pi^-}(m)$, $\sigma_{p\pi^+}(M)$ and from the angular distributions

$$\frac{dW_{\pi^+\pi^-}}{d\cos\theta} \quad \text{and} \quad \frac{dW_{p\pi^+}}{d\cos\Theta}$$

(see Eq. (A5)). Therefore, intead of the variable set y_i, the following variables are used:

$$T(t) \equiv \frac{1}{t-\mu^2} \tag{A11a}$$

$$\left(\text{note: } dT = \frac{-dt}{(t-\mu^2)^2}\right)$$

$$\sum_{\pi^+\pi^-}(m) \equiv \int_{m_a}^{m} \sigma_{\pi^+\pi^-}(m')\, dm' \tag{A11b}$$

$$\omega_{\pi^+\pi^-}(\cos\theta) \equiv \int_{-1}^{\cos\theta} \frac{dW_{\pi^+\pi^-}}{d\cos\theta}\, d\cos\theta \tag{A11c}$$

$$\sum_{p\pi^+}(M) \equiv \int_{M_a}^{M} \sigma_{p\pi^+}(M')\, dM' \tag{A11d}$$

and

$$\omega_{p\pi^+}(\cos\Theta) \equiv \int_{-1}^{\cos} \frac{dW_{p\pi^+}}{d\cos\Theta}\, d\cos\Theta \qquad \text{(A11e)}$$

Due to this change of variables a factor of 10 to 100 is saved in computer time.

Statistical Accuracy:

The number of Monte Carlo events required for a reliable calculation of the OPE cross section depends on the statistical accuracy of the cross section in each bin. Suppose we observe n events with independent weights g_i, $i = 1, \ldots,$ n in a certain bin, of say, the $p\pi^+$ mass distribution. What is the error ΔG of the cross section G,

$$G = \sum_{i=1}^{n} g_i \qquad \text{(A12)}$$

in that bin? An estimate of ΔG can be obtained as follows: The distribution of the weights g_i has a mean value

$$\bar{g} = \frac{1}{n} \sum_{i=1}^{n} g_i\,, \qquad \text{(A13)}$$

a mean square deviation

$$\Delta g^2 = \frac{1}{n-1}\left(\left(\sum g_i^2\right) - n\bar{g}^{-2}\right) \qquad \text{(A14)}$$

and an error of the mean

$$\Delta\bar{g} = \sqrt{\frac{1}{n(n-1)}\left(\left(\sum g_i^2\right) - n\bar{g}^{-2}\right)} \qquad \text{(A15)}$$

Therefore,

$$\Delta G = \Delta(n\bar{g}) = \sqrt{\frac{n}{n-1}\left(\left(\sum g_i^2\right) - \bar{g}^{-2}\right)} \simeq \sqrt{\sum g_i^2} \quad \text{for } n \gg 1. \qquad \text{(A16)}$$

REFERENCES

1. C. Goebel, Phys. Rev. Letters 1, 337 (1958);
   G. F. Chew and F. E. Low, Phys. Rev. 113, 1640 (1959);
   F. Salzmann and G. Salzmann, Phys. Rev. 120, 599 (1960);
   S. D. Drell, Phys. Rev. Letters 5, 278 (1960);
   Rev. Mod. Phys. 33, 458 (1961).
2. E. Ferrari and F. Selleri, Phys. Rev. Letters 7, 387 (1961);
   Nuovo Cimento 21, 1028 (1961);
   Suppl. Nuovo Cimento 24, 453 (1962); Nuovo Cimento 27, 1450 (1963).

3a. N. J. Sopkovich, Nuovo Cimento 26, 186 (1962);

b. M. H. Ross and G. L. Shaw, Phys. Rev. Letters 12, 627 (1964);

c. L. Durand and Y. T. Chiu, Phys. Rev. Letters 12, 399 (1964);
   Phys. Rev. 137, B1530 (1965), 139, B646 (1965);

d. K. Gottfried and J. D. Jackson, Nuovo Cimento 34, 735 (1964);

e. A. Dar and W. Tobocman, Phys. Rev. Letters 12, 511 (1964);

f. J. D. Jackson, J. T. Donohue, K. Gottfried, R. Keyser and
   B. E. Y. Svensson, Phys. Rev. 139, B428 (1965).

4. J. A. Poirier, N. N. Biswas, N. M. Cason, I. Derado, V. P. Kenney, W. D. Shepard, E. H. Synn, H. Yuta, W. Selove, R. Ehrlich, A. L. Baker, Phys. Rev. 163, 1462 (1967).
5. H. P. Dürr and H. Pilkuhn, Nuovo Cimento 40, 899 (1965).
6. G. Wolf, Phys. Rev. Letters 19, 925 (1967).
7. J. Benecke and H. P. Dürr, Nuovo Cimento 56, 269 (1968).
8. E. Colton, P. E. Schlein, E. Gellert, and G. A. Smith, University of California, Los Angeles, Report UCLA-1027 (1968).

9. Aachen-Berlin-Birmingham-Bonn-Hamburg-London (I. C.) - München collaboration, Phys. Rev. 138, B897 (1965).

10. E. Raubold, thesis, University of Hamburg, 1968, (unpublished).

11. See for example, H. Pilkuhn, The Interactions of Hadrons (North-Holland Publishing Co., Amsterdam), p. 279 ff., (1967).

12. Equation (19) gives the cross section for the OPE diagram of Fig. 3b. It has to be compared to the cross section for events with a $p\pi^+$ mass of M produced at small momentum transfers (t) between, say, target proton and the outgoing $p\pi^+$ system.

13a. G. Wolf, Phys. Letters 19, 328 (1965);

b. W. D. Walker, J. Caroll, A. Garfinkel and B. Y. Oh, Phys. Rev. Letters 18, 630 (1967);

c. J. P. Baton, G. Laurens, and J. Reignier, Phys. Letters 25B, 419 (1967);

d. E. Malamud and P. E. Schlein, Phys. Rev. Letters 19, 1056 (1967).

14. $\bar{p}p \rightarrow \bar{\Delta}^{++}\Delta^{++}$:

a. H. C. Dehne, E. Raubold, P. Söding, M. W. Teucher, G. Wolf, and E. Lohrmann, Phys. Letters 9, 185 (1964), and H. C. Dehne, University of Hamburg, thesis, 1964 (unpublished), (3.6 GeV/c);

b. Bonn-Hamburg-Milano collaboration, Phys. Letters 15, 356 (1966), (5.7 GeV/c);

c. V. Alles-Borelli, B. French, A. Frisk, and L. Michejda, Nuovo Cimento 48, 360 (1967), (5.7 GeV/c).

15. $pp \rightarrow \Delta^{++}n$:

a. S. Coletti, J. Kidd, L. Mandelli, V. Pelosi, S. Ratti, V. Russo, L. Tallone, E. Zampieri, C. Caso, F. Conte, M. Dameri, C. Crosso, and G. Tomassini, Nuovo Cimento 49, 479 (1967), (4.0 GeV/c).

b. H. C. Dehne, J. Diaz, K. Strömer, A. Schmitt, W. P. Swanson, and G. Wolf, Nuovo Cimento 53, 232 (1968), (10.0 GeV/c).

16. $\pi^+ p \rightarrow \Delta^{++} \rho^o$:

a. N. Gelfand, Columbia University, NEVIS report 137, June 1965, unpublished (2.35 GeV/c); The data at 3-4 GeV/c and 6.95 GeV/c have been taken from

b. D. Brown, G. Gidal, R. W. Birge, R. Bacastow, S. Yiu Fung, W. Jackson and R. Pu, Phys. Rev. Letters 19, 664 (1967);

c. P. Slatterly, H. Kraybill, B. Forman, and T. Ferbel, University of Rochester Report UR-875-153, July 1966, unpublished, (6.95 GeV/c);

d. Aachen-Berlin-Birmingham-Bonn-Hamburg-London (I.C.) - München collaboration, Nuovo Cimento 35, 659 (1965); and

e. Phys. Rev. 138, B897 (1965), (4.0 GeV/c);

f. J. Ballam, A. Brody, G. Chadwick, Z.G.T. Guiragossian, W. B. Johnson, R. R. Larsen, D.W.G.S. Leith, and E. Pickup, private communication, (16.0 GeV/c).

17. $\pi^- p \rightarrow n\rho^o$:

a. Saclay-Orsay-Bari-Bologna collaboration, Nuovo Cimento 29, 515 (1963), (1.59 GeV/c); and

b. Preprint, 1964, and Nuovo Cimento 35, 713 (1965), (2.75 GeV/c);

c. J. A. Poirier, N. N. Biswas, N. M. Caso, I. Derado, V. P. Kenney, W. D. Shephard, E. H. Synn, H. Yuta, W. Selove, R. Ehrlich, and A. L. Baker, Phys. Rev. 163, 1462 (1967), (8.0 GeV/c).

18. E. Clementel and C. Villi, Nuovo Cimento 4, 1207 (1956).

19. This value of $\langle r_p^2 \rangle^{1/2}$ was obtained from a straight line fit to the values of the electric form factor of the proton as measured at momentum transfers below $1f^{-2}$ by B. Dudelzak, G. Sauvage, and P. Lehmann, Nuovo Cimento 28, 18 (1962), and T. Janssens, R. Hofstadter, E. B. Hughes, and M. R. Yearian, Phys. Rev. 142, 922 (1966).

20. W. Bartel, B. Dudelzak, H. Krehbiel, J. McElroy, U. Meyer-Berkhout, W. Schmidt, V. Walther and G. Weber, Phys. Letters 27B, 660 (1968).

21. A. Donnachie, R. G. Kirsopp, and C. Lovelace, CERN TH 838, (1967).

22. Aachen-Birmingham-Bonn-Hamburg-London (I. C.) - München collaboration
   a. Nuovo Cimento 31, 485 (1964);
   b. Nuovo Cimento 31, 729 (1964).

23. See for example:
   Geneva-Hamburg-Milano-Saclay collaboration, Nuovo Cimento 54, 983 (1968);
   C. Baltay, H. H. Kung, N. Yeh, T. Ferbel, P. F. Slatterly, M. Rabin, H. L. Kraybill, Phys. Rev. Letters 20, 887 (1968);
   T. F. Johnston, J. D. Prentice, N. R. Steenberg, T. S. Yoon, A. F. Garfinkel, R. Morse, B. Y. Oh, W. D. Walker, Phys. Rev. Letters 20, 1414 (1968).

24. N. Schmitz, Nuovo Cimento 31, 255 (1964).

25. Saclay-Orsay-Bari-Bologna collaboration, Nuovo Cimento 35, 1 (1965).

26. Genova-Hamburg-Milano-Saclay collaboration, Nuovo Cimento 57, 699 (1968).

27. Genova-Hamburg-Milano-Saclay collaboration, private communication by P. v. Handel.

28. The program OPEM evolved out of a Monte Carlo program originally written by P. Söding.

29. F. E. James and H. L. Kraybill, Bull. Am. Phys. Soc. 8, 342 (1963), and Yale University preprint, 1963.

30. Columbia-Rutgers collaboration, private communication by C. Baltay.

31. P. H. Satterblom, W. D. Walker, and A. R. Erwin, Phys. Rev. 134, B207 (1964).

32. J. W. Lamsa, N. M. Cason, N. N. Biswas, I. Derado, T. H. Groves, V. P. Kenney, J. A. Poirier, and W. D. Shephard, Phys. Rev. 166, 1395 (1968).

33. Genova-Hamburg-Milano-Saclay collaboration, Nuovo Cimento 47A, 675 (1967).

34. M. L. Ioffredo, G. W. Brandenburg, A. E. Brenner, B. Eisenstein, L. Eisenstein, W. H. Johnson, Jr., J. K. Kim, M. E. Law, B. M. Salzberg, J. H. Scharenguivel, L. K. Sisterson, and J. J. Szymanski; Contribution to the XIVth International Conference on High-Energy Physics, Vienna, 1968; and private communication.

35a. G. F. Chew and A. Pignotti, Phys. Rev. Letters 20, 1078 (1968).

b. R. T. Deck, Phys. Rev. Letters 13, 169 (1964).

36. M. N. Focacci and G. Giacomelli, CERN-Report 66-18, 1966, unpublished.

37. J. T. Lach, University of California Radiation Laboratory Report UCRL-10718, 1963 (unpublished).

38. J. A. Helland, T. J. Devlin, D. E. Hagge, M. J. Longo, B. J. Moyer, and C. D. Wood, Phys. Rev. 134, B1062 (1964).

39. P. Bareyre, C. Brickman, and G. Villet, Phys. Rev. 165, 1730 (1968).

TABLE I: R parameters and rms radii $\langle r^2 \rangle^{1/2}$ as obtained from fits to the momentum transfer distributions.

	Vertex	R (GeV^{-1})	R (f)	$\langle r^2 \rangle^{1/2}$ (f)
R_N	$NN\pi$	2.86 ± 0.08	0.57 ± 0.02	1.06 ± 0.04
R_Δ	$\Delta N\pi$	1.76 ± 0.03	0.35 ± 0.01	0.86 ± 0.02
R_ρ	$\rho\pi\pi$	2.31 ± 0.19	0.46 ± 0.04	0.65 ± 0.05
R_{S11}	S11 $N\pi$	0.03	0.	0.
R_{P11}	P11 $N\pi$	0.34 fixed	0.1	0.14
R_{D13}	D13 $N\pi$	4.5 fixed	0.9	0.9
R_{D15}	D15 $N\pi$	5.5		
R_{F15}	F15 $N\pi$	4.5 fixed	0.9	0.8
R_{F17}	F17 $N\pi$	4.5 fixed	0.9	
R_{F37}	F37 $N\pi$	4.5 fixed	0.9	0.7
R	$(\pi\pi)^{T=0}(\pi\pi)$	0.01	0.	0.
R_f	$f\,\pi\pi$	3.23 ± 1.46	.65 ± .29	0.58 ± 0.26
R_g	$g\,\pi\pi$	4.5 fixed	0.9	0.5
R_{20}	$(\pi\pi)^{T=2,\ \ell=0}(\pi\pi)$	0.0 ± 0.01	0.	0.
R_{22}	$(\pi\pi)^{T=2,\ \ell=2}(\pi\pi)$	3.59 ± 1.19	0.72 ± 0.24	0.72 ± 0.24
R_{24}	$(\pi\pi^{T=2,\ \ell=4}(\pi\pi)$	4.5 fixed	0.9	0.6

TABLE II: Results from the Regge fits.

a) $$\frac{d\sigma_i^{Regge}}{dt} = \frac{d\sigma^{OPE}}{dt}\, d_i(t)\, s^{2\,\alpha(t)}$$

i = 1, ..., 4 for the reactions (1), ..., (4)

$-t$ (GeV^2)	$\alpha(t)$	$d_1(t)$	$d_2(t)$	$d_3(t)$	$d_4(t)$
0 - 0.1	0.060 ± 0.040	0.67 ± 0.14	0.78 ± 0.13	0.70 ± 0.13	0.79 ± 0.12
0.1 - 0.2	0.0 ± 0.013	0.9 ± 0.2	1.04 ± 0.07	1.11 ± 0.15	1.04 ± 0.09
0.2 - 0.3	0.0 ± 0.078	1.06 ± 0.41	1.00 ± 0.33	1.10 ± 0.43	1.08 ± 0.29
0.3 - 0.4	-0.810^{-4} ± 0.15	1.20 ± 0.90	0.88 ± 0.55	1.08 ± 0.75	0.84 ± 0.42
0.4 - 0.5	0.0 ± 0.21	0.98 ± 0.97	0.85 ± 0.72	0.98 ± 0.93	---
0.5 - 0.6	0.03 ± 0.37	0.95 ± 1.7	1.01 ± 1.57	0.67 ± 1.16	---

b) $$\frac{d\sigma_i^{Regge}}{dt} = \frac{d\sigma_i^{OPE}}{dt}\, d_i \left(\frac{s}{s_{oi}}\right)^{2\alpha'(0)(t-\mu^2)}$$

i = 1, ..., 4 for the reactions (1), ..., (4)

$\alpha' = -(0.051 \pm 0.062)GeV^{-2}$

s_{01}	$= (0.58 \pm 1.1)GeV^2$	d_{01}	$= 0.90 \pm 0.044$
s_{02}	$= (2.9 \pm 2.4)GeV^2$	d_{02}	$= 1.00 \pm 0.049$
s_{03}	$= (1.5 \pm 1.5)GeV^2$	d_{03}	$= 0.96 \pm 0.060$
s_{04}	$= (1.3 \pm 1.4)GeV^2$	d_{04}	$= 0.98 \pm 0.050$

TABLE III: Comparison of observed (σ^{exp}) and OPE predicted (σ^{OPE}) cross sections. The contributions of the OPE diagrams (a) - (f) shown in Fig. 1 are given separately.

a) $\pi^+ p \longrightarrow p\pi^+\pi^+\pi^-$.

beam momentum (GeV/c)	σ^{exp} (mb)	σ^{OPE}(mb) (a)+(b)	(c)	total
1.95	3.64 ± 0.20 [29]	1.47	0.08	1.55
4.0	3.13 ± 0.07 [16e]	1.80	0.17	1.97
8.5	2.3 [30]	1.29	0.23	1.52
16	1.28 ± 0.15 [16f]	0.93	0.24	1.17

b) $\pi^- p \longrightarrow p\pi^+\pi^-\pi^-$

beam momentum (GeV/c)	σ^{exp} (mb)	σ^{OPE}(mb) (d)+(e)	(f)	total
1.59	0.88 ± 0.04 [17a]	0.13	0.44	0.57
2.1	1.67 ± 0.08 [31]	0.22	0.45	0.67
2.75	1.83 ± 0.05 [17b]	0.34	0.50	0.84
4.0	1.95 ± 0.10 [22]	0.60	0.57	1.17
8.05	1.27 ± 0.07 [32]	0.62	0.51	1.13
11	1.3 ± 0.1 [33]	0.59	0.46	1.05
16	1.08 ± 0.15 [16f]	0.55	0.42	0.97
20	0.89 ± 0.06 [34]	0.53	0.39	0.92

TABLE IV: Coefficients d_n of $\pi\pi$ Angular Distributions

$$(dW/d\cos\theta = \sum d_n \cos\theta^n)$$

a) $\pi^+\pi^- \longrightarrow \pi^+\pi^-$

m (GeV)	d_0	d_1	d_2	d_3	d_4
0.28 - 0.4	0.5				
0.4 - 0.5	0.42	0.10	0.24		
0.5 - 0.6	0.35	0.21	0.45		
0.6 - 0.7	0.36	0.30	0.42		
0.7 - 0.8	0.27	0.38	0.69		
0.8 - 0.9	0.35	0.26	0.45		
0.9 - 1.0	0.37	0.17	0.39		
1.0 - 1.1	0.27	-0.10	0.69		
1.1 - 1.2	0.65	0	-2.82	0	3.95
1.2 - 1.3	0.21	0	-1.95	0	4.70
1.3 - 1.4	0.21	0	-1.95	0	4.70

b) $\pi^\pm\pi^\pm \longrightarrow \pi^\pm\pi^\pm$

m (GeV)	d_0	d_2	d_4
0.28 - 0.8	0.5		
0.8 - 1.0	0.31	0.48	0.15
1.0 - 1.2	0.30	0.18	0.70
1.2 - 1.4	0.30	-0.36	1.60

FIGURE CAPTIONS

1. a) - c) The three OPE diagrams for the reaction $\pi^+ p \rightarrow p\pi^+\pi^+\pi^-$.

   d) - f) The three OPE diagrams for the reaction $\pi^- p \rightarrow p\pi^+\pi^-\pi^-$.

2. Approximation of the scattering process $a + b \rightarrow a' + b'$ by the exchange of a scalar particle x with mass m_x.

3. OPE diagrams for the reactions $\bar{p}p \rightarrow \bar{\Delta}^{++}\Delta^{++}$ (a), $pp \rightarrow \Delta^{++}n$ (b), $\pi^+ p \rightarrow \Delta^{++}\rho^0$ (c), $\pi^- p \rightarrow n\rho^0$ (d).

4. Differential cross sections $d\sigma/d|t|$ for events of reaction (1) in the $\bar{\Delta}^{++}$, Δ^{++} mass region. The curves give the result of the OPE fit.

   a) at 3.6 GeV/c[14a] (1.13 GeV < $M_{\bar{\Delta},\Delta}$ < 1.33 GeV)

   b) at 5.7 GeV/c[14c] (1.15 GeV < $M_{\bar{\Delta},\Delta}$ < 1.35 GeV).

5. Differential cross sections $d\sigma/d|t|$ for events of reaction (2) in the Δ^{++} region. The curves give the result of the OPE fit.

   a) at 4 GeV/c[15a] (1.08 GeV < M < 1.40 GeV)

   b) at 10 GeV/c[15b] (1.125 < M < 1.325 GeV).

6. Differential cross sections $d\sigma/d|t|$ for events of reaction (3) in the Δ^{++}, ρ^0 region. The curves in a) - d) give the result of the OPE fit. The curve for the 16 GeV/c case, (e), is a prediction of the OPE model.

   a) at 2.35 GeV/c[16a] (0.675 GeV < m < 0.825 GeV, 1.185 GeV < M < 1.285 GeV).

   b) at 3 - 4 GeV/c[16b] (0.68 GeV < m < 0.86 GeV, 1.12 GeV < M < 1.32 GeV).

   c) at 4 GeV/c[16d] (0.66 GeV < m < 0.86 GeV, 1.12 GeV < M < 1.32 GeV).

   d) at 6.95 GeV/c[16c] (0.64 GeV < m < 0.88 GeV, 1.12 GeV < M < 1.42 GeV).

   e) at 16 GeV/c[16f] (0.68 GeV < m < 0.86 GeV, 1.12 GeV < M < 1.32 GeV.

7. Differential cross sections $d\sigma/d|t|$ for events of reaction (4) in the ρ^0 region. The curves give the results of the OPE fit.
   a) at 1.59 GeV/c[17a] (0.616 GeV < m < 0.85 GeV)
   b) at 2.75 GeV/c[17b] (0.65 GeV < m < 0.85 GeV)
   c) at 8.0 GeV/c[17c] (0.675 GeV < m < 0.875 GeV).
8. The 33 πN phase shift δ_{33} as a function of the πN cm energy M. The data are taken from Ref. 21. The curve is the result of a fit with the BD parametrization.
9. The effective Regge trajectory $\alpha(t)$ for the reactions (1) - (4) as obtained from the fit discusses in Section V.
10. The differential cross sections $d\sigma/d|t|$ for the events of the reaction $\pi^- p \rightarrow n f^0$. The curves give the result of the OPE fit.
   a) at 4 GeV/c[22] (1.16 GeV < m < 1.38 GeV)
   b) at 8 GeV/c[4] (1.17 GeV < m < 1.37 GeV)
   The differential cross section $d\sigma/d|t|$ for the events of the reaction $\pi^- p \rightarrow n g^0$. The curve gives the result of the OPE fit.
   c) at 8 GeV/c[4] (1.60 GeV < m < 1.75 GeV).
11. Differential cross sections $d\sigma/d|t|$ for events of the reaction 11 GeV/c $\pi^- p \rightarrow \Delta^{++} \pi^- \pi^-$[27] (1.12 GeV < M < 1.34 GeV) for different $\pi^-\pi^-$ mass intervals. The curves give the result of the OPE fit.
12. Differential cross section $d\sigma/d|t|$ for events of the reaction 16 GeV/c $\pi^- p \rightarrow \Delta^{++} \pi^- \pi^-$[16f] (1.16 GeV < M < 1.32 GeV) for different $\pi^-\pi^-$ mass intervals. The curves give the result of the OPE fit.
13. The elastic differential cross section $\sigma_{\pi^\pm\pi^\pm}(m)$ for $\pi^\pm\pi^\pm$ scattering as deduced from experimental data for the reactions 4.0 GeV/c $\pi^+ p \rightarrow \pi^+ \pi^+ n$[16e] (-⊹-), 11 GeV/c $\pi^- p \rightarrow \Delta^{++} \pi^- \pi^-$[27] (-⊹-) and 16 GeV/c $\pi^- p \rightarrow \Delta^{++} \pi^- \pi^-$[16f] (-+-).

14. Effective mass distributions for the reaction 1.95 GeV/c $\pi^+ p \longrightarrow p\pi^+\pi^+\pi^-$[29]. The curves show the predictions of the OPE model.

a) $p\pi^+$

b) $p\pi_a^+$ for events with $|t|_{p/p\pi^+_a} < 0.6$ GeV^2

c) $\pi_b^+\pi^-$ for events with $p\pi_a^+$ in the Δ region (1.12 GeV $< M_{p\pi_a^+} < 1.32$ GeV) and $|t|_{p/p\pi_a^+} < 0.6$ GeV^2.

15. Effective mass distributions for the reaction 4 GeV/c $\pi^+ p \longrightarrow p\pi^+\pi^+\pi^-$[16e]. The curves show the predictions of the OPE model.

a) $p\pi^+$

b) $p\pi^-$

c) $\pi^+\pi^-$

d) $\pi^+\pi^+$

e) $p\pi_a^+$ for events with $\pi_b^+\pi^-$ in the ρ region (0.66 GeV $< M_{\pi_b^+\pi^-} < 0.86$ GeV) and $|t|_{p/p\pi_a^+} < 0.3$ GeV^2.

f) $\pi_b^+\pi^-$ for events with $p\pi_a^+$ in the Δ region (1.12 GeV $< M_{p\pi_a^+} < 1.32$ GeV) and $|t|_{p/p\pi_a^+} < 0.3$ GeV^2.

16. Effective mass distributions for the reaction 8.5 GeV/c $\pi^+ p \longrightarrow p\pi^+\pi^+\pi^-$[30] for events with $p_p^{lab} < 1$ GeV (p_p^{lab} proton momentum in the laboratory system). The curves show the predictions of the OPE model.

a) $p\pi^+$

b) $p\pi_a^+$ for events with $\pi_b^+\pi^-$ in the ρ^o region (0.66 GeV $< M_{\pi_b^+\pi^-} < 0.86$ GeV)

c) $\pi^+\pi^-$

d) $\pi_b^+\pi^-$ for events with $p\pi_a^+$ in the Δ^{++} region (1.136 GeV $< M_{p\pi_a^+} < 1.336$ GeV)

17. Effective mass distributions for the reaction 16 GeV/c $\pi^+ p \longrightarrow p\pi^+\pi^+\pi^-$[16f].

The curves show the predictions of the OPE model.

a) $p\pi^+$

b) $p\pi^+_a$ for events with $\pi^+_a\pi^-$ in the ρ region (0.62 GeV < $M_{\pi^+_b\pi^-}$ < 0.92 GeV).

c) $\pi^+\pi^-$

d) $\pi^+_b\pi^-$ for events with $p\pi^+_a$ in the Δ region (1.08 GeV < $M_{p\pi^+_a}$ < 1.40 GeV).

18. Effective mass distributions for the reaction 2.1 GeV/c $\pi^- p \longrightarrow p\pi^+\pi^-\pi^-$[31].

The curves show the predictions of the OPE model.

a) $p\pi^+$

b) $p\pi^-$

c) $\pi^+\pi^-$

19. Effective mass distributions for the reaction 4 GeV/c $\pi^- p \longrightarrow p\pi^+\pi^-\pi^-$[22b]. The curves show the predictions of the OPE model.

a) $p\pi^+$

b) $p\pi^-$

c) $\pi^+\pi^-$

d) $\pi^-\pi^-$

20. Effective mass distributions for the reaction 8.05 GeV/c $\pi^- p \longrightarrow p\pi^+\pi^-\pi^-$[32].

The curves show the predictions of the OPE model.

a) $p\pi^+$

b) $p\pi^-$

c) $\pi^+\pi^-$

21. Effective mass distributions for the reaction 11 GeV/c $\pi^- p \longrightarrow p\pi^+\pi^-\pi^-$[33].

The curves show the predictions of the OPE model.

a) $p\pi^+$

b) $p\pi^+\pi^-$

22. Effective mass distributions for the reaction 13 GeV/c $\pi^- p \rightarrow p\pi^+\pi^-\pi^-$[34].

The curves show the predictions of the OPE model.

a) $p\pi^+$

b) $p\pi^-$

c) $\pi^+\pi^-$

d) $p\pi^+\pi_a^-$ for events with $\pi^+\pi_b^-$ not in the ρ region ($0.66\ \text{GeV} < M_{\pi^+\pi_b^-} < 0.86\ \text{GeV}$).

e) $p\pi^+\pi_a^-$ for events with $p\pi^+$ in the Δ region ($1.15\ \text{GeV} < M_{p\pi^+} < 1.35\ \text{GeV}$) and $\pi^+\pi_a^-$ not in the ρ region ($0.66\ \text{GeV} < M_{\pi^+\pi_a^-} < 0.86\ \text{GeV}$).

f) $p\pi_a^-$ for events with $\pi^+\pi_b^-$ in the ρ region ($0.66\ \text{GeV} < M_{\pi^+\pi_b^-} < 0.86\ \text{GeV}$), $p\pi^+$ outside Δ region ($1.15\ \text{GeV} < M_{p\pi^+} < 1.35\ \text{GeV}$), and $|t|_{p/p\pi_a^-} < 0.2\ \text{GeV}^2$.

g) $p\pi_a^-$ for events with $\pi^+\pi_a^-$ not in the ρ region ($0.66\ \text{GeV} < M_{\pi^+\pi_a^-} < 0.86\ \text{GeV}$), $p\pi^+$ outside Δ region ($1.15\ \text{GeV} < M_{p\pi^+} < 1.35\ \text{GeV}$), and $|t|_{p/p\pi_a^-} < 0.2\ \text{GeV}^2$.

h) $\pi^+\pi^-$ for events with $p\pi^+$ not in the Δ region ($1.15\ \text{GeV} < M_{p\pi^+} < 1.35\ \text{GeV}$), and $\pi^+\pi^-\pi^-$ not in the A region ($M_{\pi^+\pi^-\pi^-} < 1.4\ \text{GeV}$)

23. Effective mass distributions for the reaction 16 GeV/c $\pi^- p \rightarrow p\pi^+\pi^-\pi^-$[16f].

The curves show the predictions of the OPE model

a) $p\pi^+$

b) $p\pi^+$ for events with $|t|_{p/p\pi^+} < 0.25\ \text{GeV}^2$.

c) $p\pi^-$

d) $p\pi^-$ for events with $|t|_{p/p\pi^-} < 0.25\ \text{GeV}^2$

e) $\pi^+\pi^-$

f) $\pi^-\pi^-$

g) $p\pi^+\pi^-$ for events with $|t|_{p/p\pi^+\pi^-} < 0.25\ \text{GeV}^2$

h) $p\pi^+\pi^-$

24. Effective mass distributions for the reaction 20 GeV/c $\pi^- p \rightarrow p\pi^+\pi^-\pi^-$[34].

The curves show the predictions of the OPE model.

a) $p\pi^+$

b) $p\pi^-$

c) $p\pi^+\pi^-$

d) $\pi^+\pi^-$

e) $\pi^-\pi^-$

25. Momentum transfer distributions $d\sigma/d|t|$ from events of the reaction $\pi^- p \rightarrow p\pi^+\pi^-\pi^-$[34]. The curves show the predictions of the OPE model.

a) Distribution of the square of the four momentum transfer, $|t|_{p/\Delta^{++}}$ for events with $p\pi^+$ in the Δ region ($1.15\ \text{GeV} < M_{p\pi^+} < 1.35\ \text{GeV}$) and $\pi^+\pi^-$ not in the ρ region ($0.66\ \text{GeV} < M_{\pi^+\pi^-} < 0.86\ \text{GeV}$) at 13 GeV/c.

b) same as a) at 20 GeV/c.

c) Distribution of the square of the four momentum transfer, $|t|_{\pi^-/\rho^0}$ for events with $\pi^+\pi^-$ in the ρ region ($0.66\ \text{GeV} < M_{\pi^+\pi^-} < 0.86\ \text{GeV}$) and $p\pi^+$ not in the Δ region ($1.15\ \text{GeV} < M_{p\pi^+} < 1.35\ \text{GeV}$) at 13 GeV/c.

d) Same as b) at 20 GeV/c.

26. The elastic cross sections

a) for $p\pi^+$ scattering

b) for $p\pi^-$ scattering

c) for $\pi^+\pi^-$ scattering

d) for $\pi^\pm\pi^\pm$ scattering

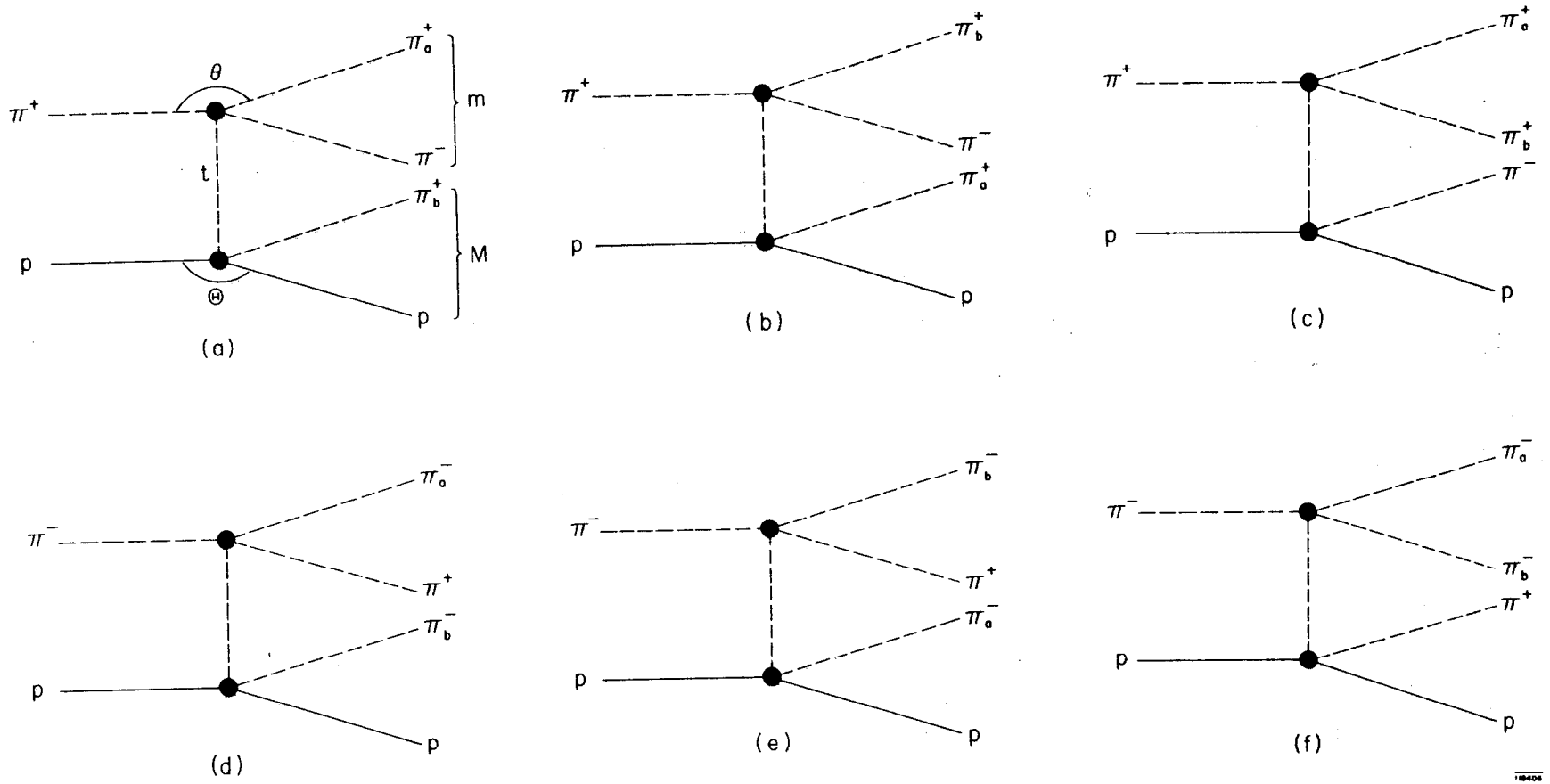
π^+
θ
π_a^+
m
π^-
t
π_b^+
p
M
Θ
p
(a)
π^+
π_b^+
π^-
π_a^+
p
p
(b)
π^+
π_a^+
π_b^+
π^-
p
p
(c)
π^-
π_a^-
π^+
π_b^-
p
p
(d)
π^-
π_b^-
π^+
π_a^-
p
p
(e)
π^-
π_a^-
π_b^-
π^+
p
p
(f)

Fig. 1

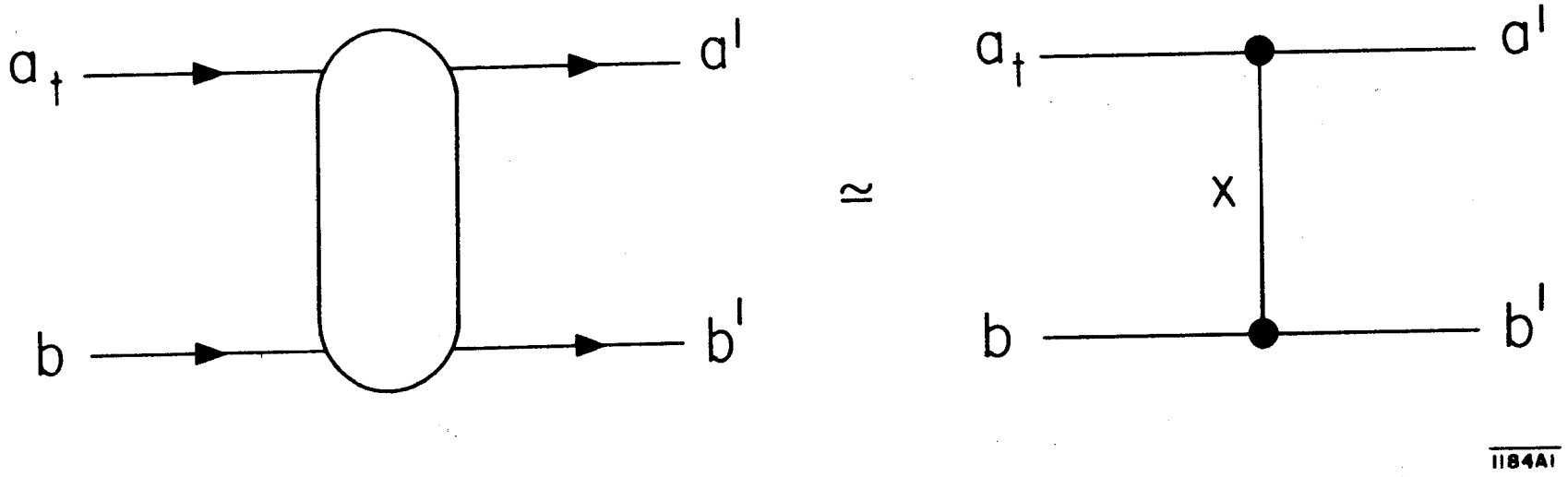

Fig. 2

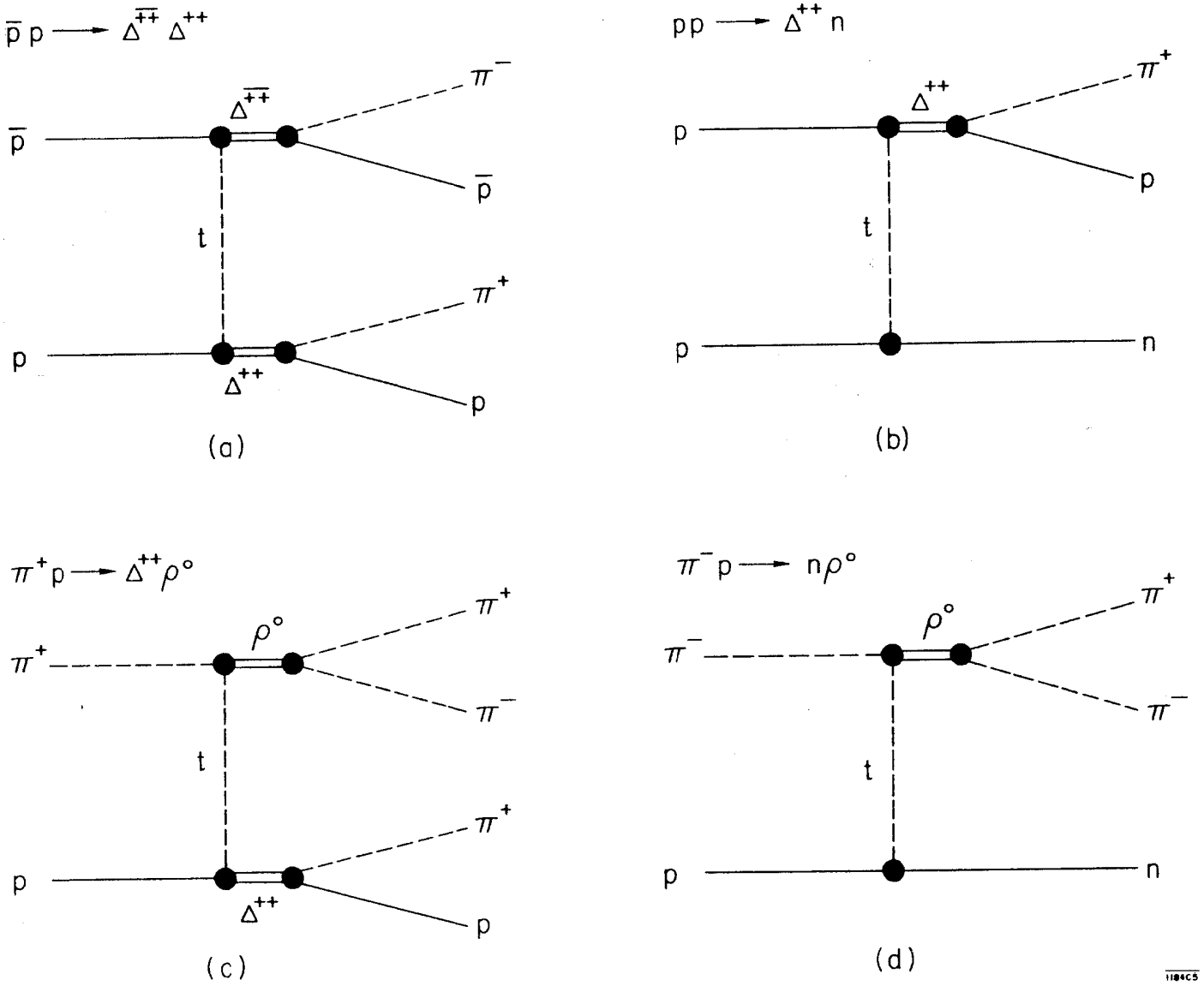
$\bar{p}\,p \longrightarrow \Delta^{\bar{++}}\,\Delta^{++}$
$\bar{p}$
$\Delta^{\bar{++}}$
π^-
$\bar{p}$
t
π^+
p
Δ^{++}
p
(a)
$pp \longrightarrow \Delta^{++}\,n$
π^+
p
Δ^{++}
p
t
p
n
(b)
$\pi^+ p \longrightarrow \Delta^{++}\rho^\circ$
π^+
ρ°
π^+
π^-
t
π^+
p
Δ^{++}
p
(c)
$\pi^- p \longrightarrow n\rho^\circ$
π^+
ρ°
π^-
π^-
t
p
n
(d)
1184C5

Fig. 3

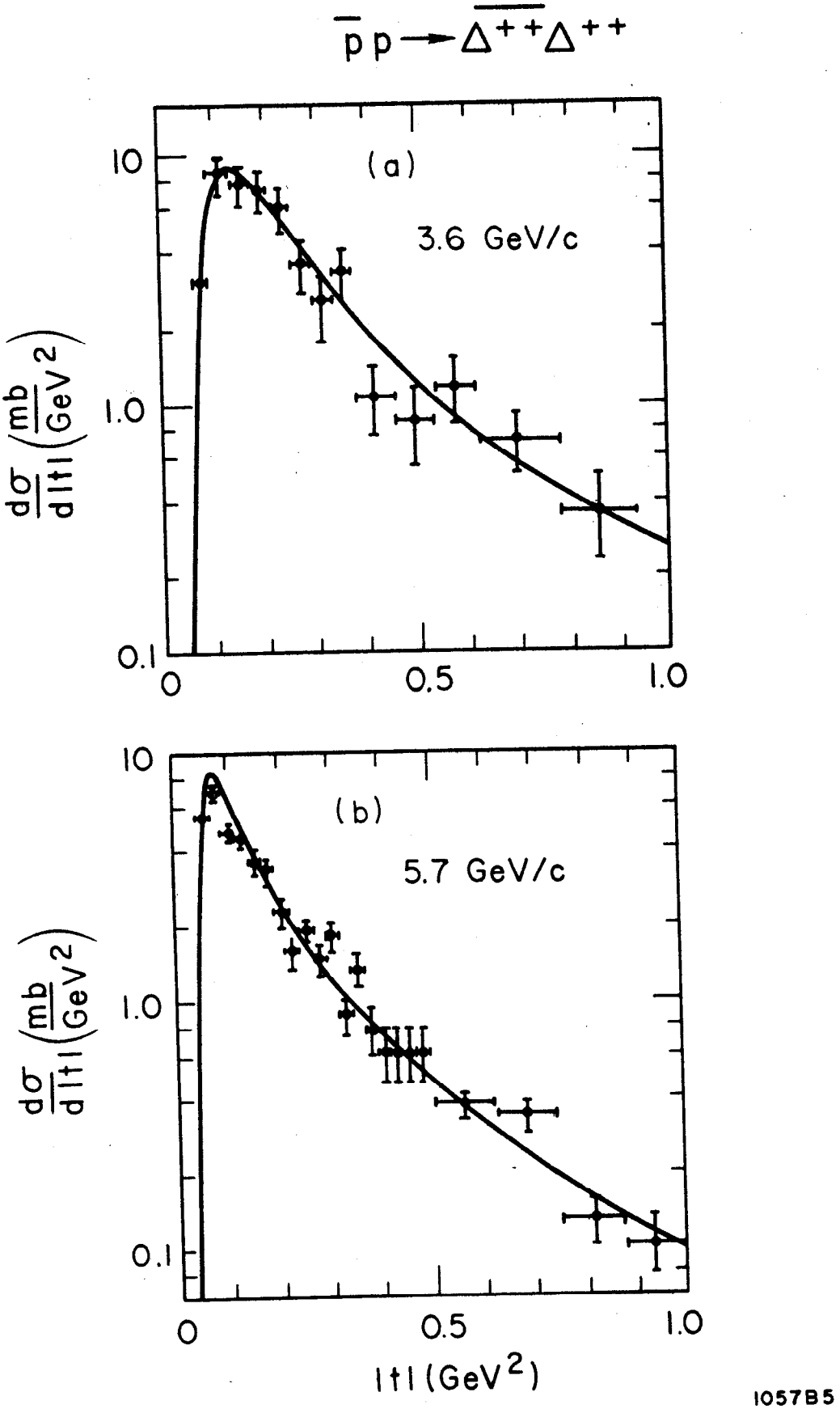
$\bar{p}p \rightarrow \overline{\Delta^{++}}\Delta^{++}$
(a)
3.6 GeV/c
(b)
5.7 GeV/c
$\frac{d\sigma}{d|t|}\left(\frac{mb}{GeV^2}\right)$
10
1.0
0.1
0
0.5
1.0
$|t|\,(GeV^2)$
1057B5

Fig. 4

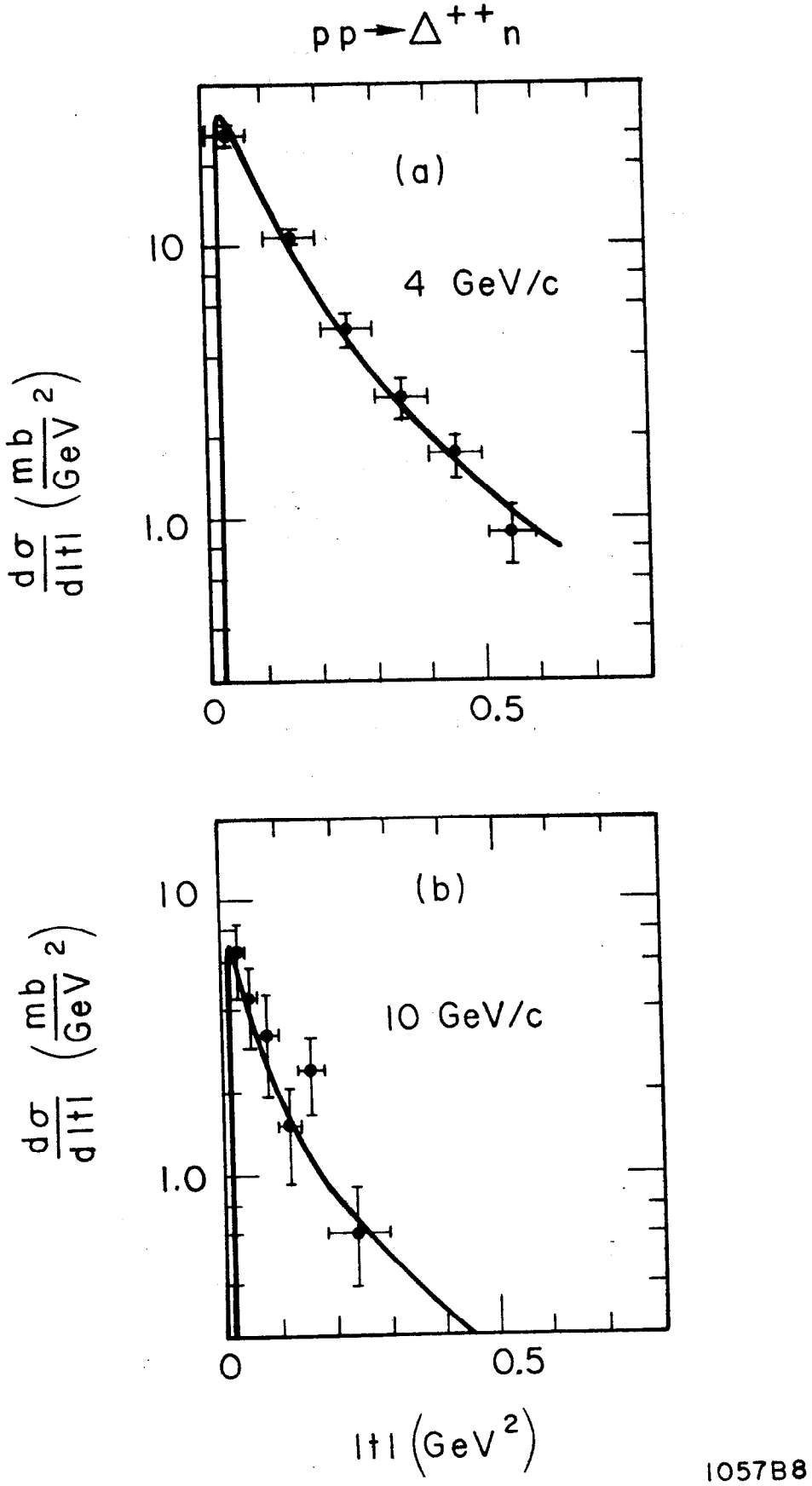
pp→Δ++n
(a)
4 GeV/c
10
1.0
0
0.5
dσ/d|t| (mb/GeV²)
(b)
10 GeV/c
10
1.0
0
0.5
dσ/d|t| (mb/GeV²)
|t| (GeV²)

1057B8

Fig. 5

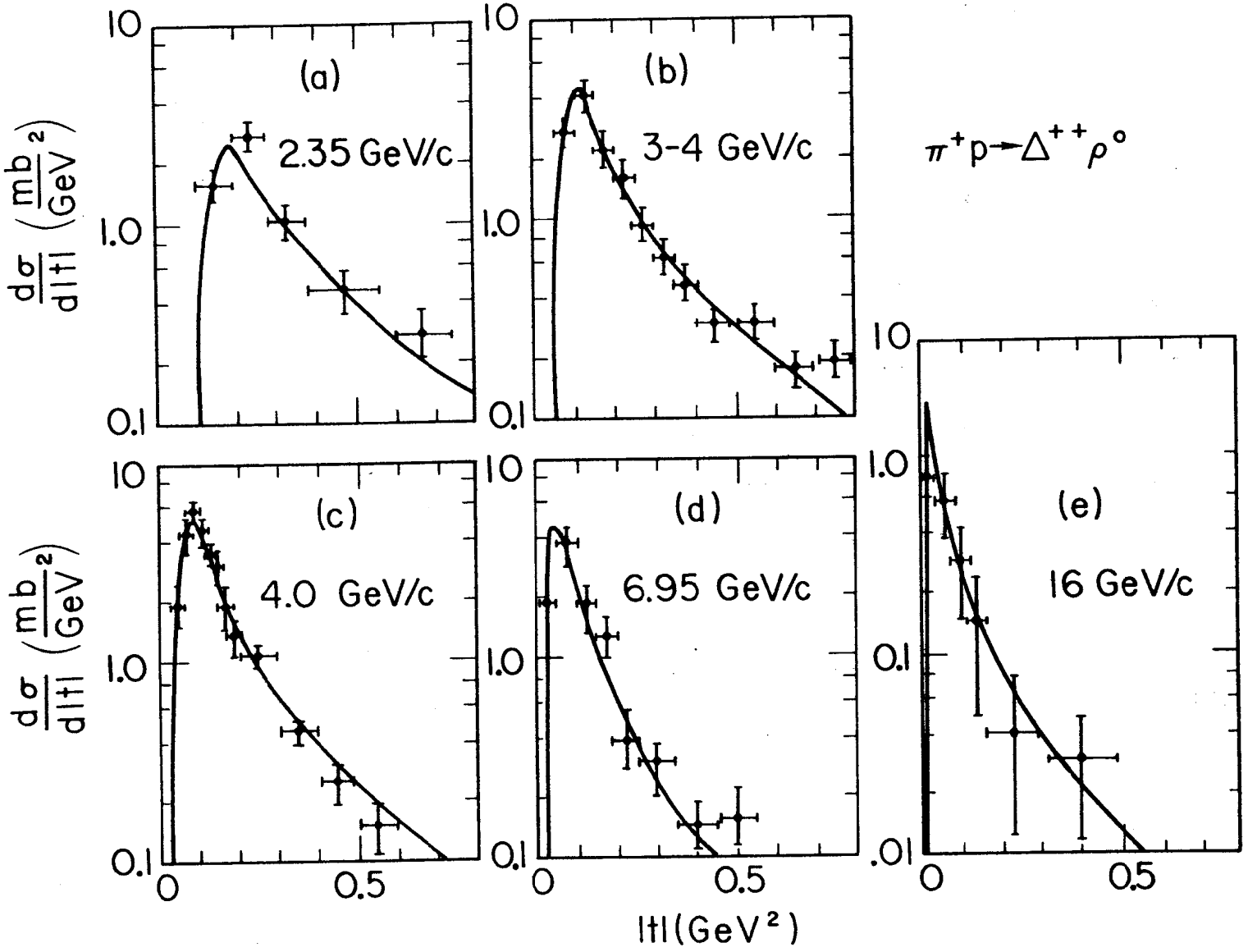
(a)
2.35 GeV/c
(b)
3-4 GeV/c
(c)
4.0 GeV/c
(d)
6.95 GeV/c
(e)
16 GeV/c
$\pi^+ p \to \Delta^{++} \rho^0$
$\frac{d\sigma}{d|t|}\left(\frac{mb}{GeV^2}\right)$
$|t|(GeV^2)$
10
1.0
0.1
.01
0
0.5
1057C6

Fig. 6

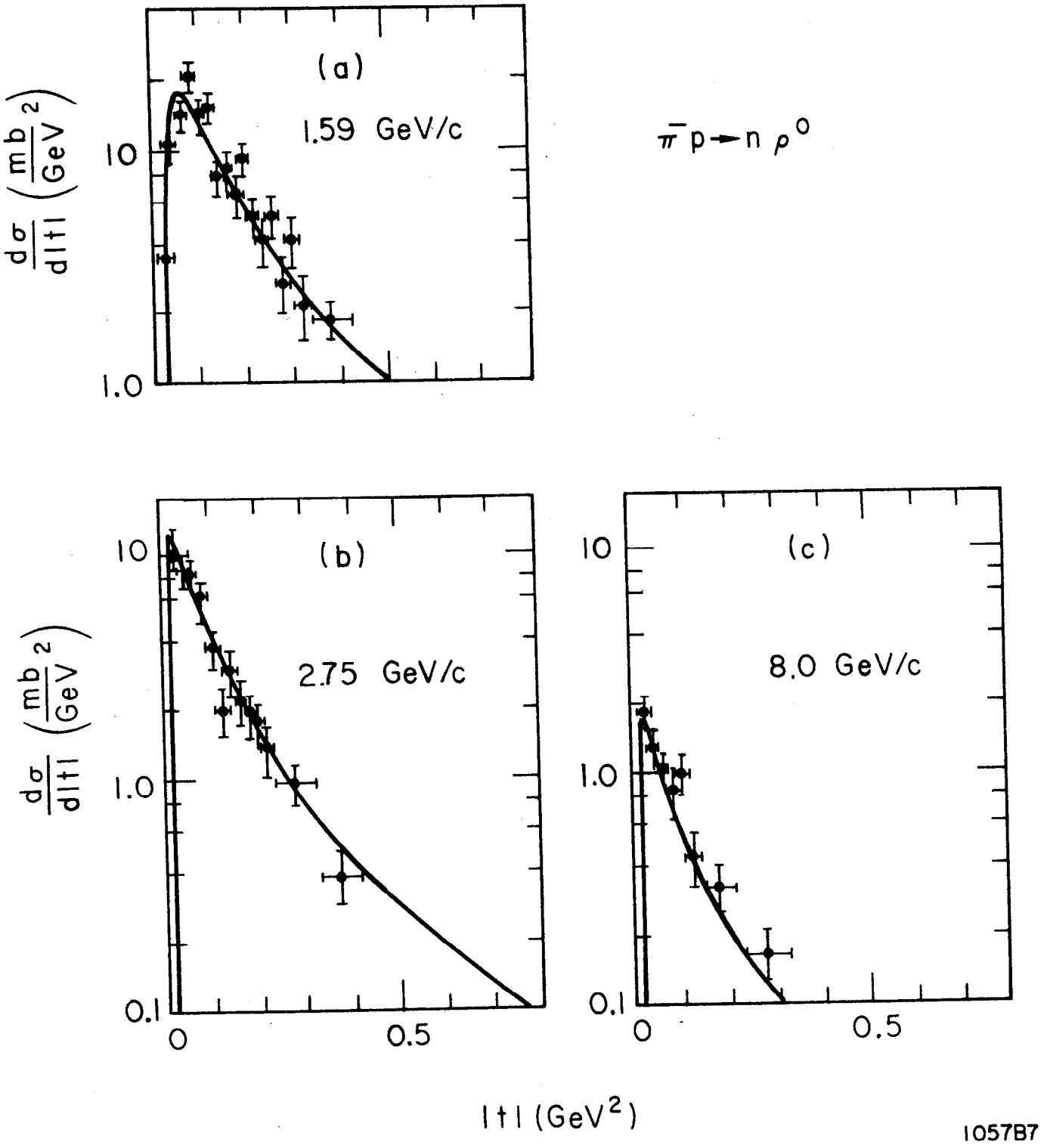
(a)
1.59 GeV/c
(b)
2.75 GeV/c
(c)
8.0 GeV/c
$\pi^- p \to n \rho^0$
$\frac{d\sigma}{dt}\left(\frac{mb}{GeV^2}\right)$
10
1.0
0.1
0
0.5
$|t|\ (GeV^2)$
1057B7

Fig. 7

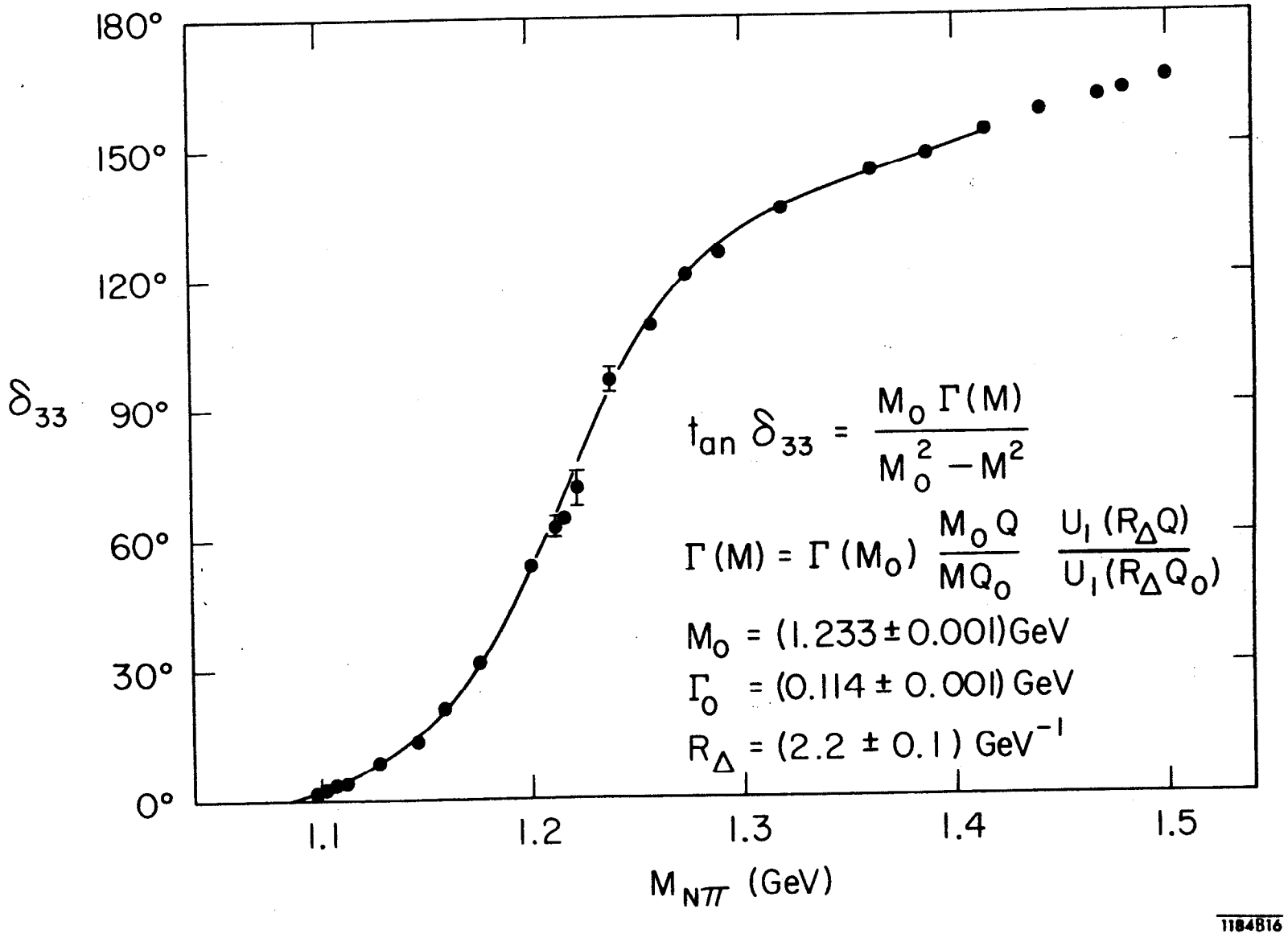
180°
150°
120°
90°
60°
30°
0°
δ_{33}
1.1
1.2
1.3
1.4
1.5
$M_{N\pi}$ (GeV)
$\tan \delta_{33} = \frac{M_0 \Gamma(M)}{M_0^2 - M^2}$
$\Gamma(M) = \Gamma(M_0) \frac{M_0 Q}{M Q_0} \frac{U_1(R_\Delta Q)}{U_1(R_\Delta Q_0)}$
$M_0 = (1.233 \pm 0.001)$ GeV
$\Gamma_0 = (0.114 \pm 0.001)$ GeV
$R_\Delta = (2.2 \pm 0.1)$ GeV^{-1}
1184816

Fig. 8

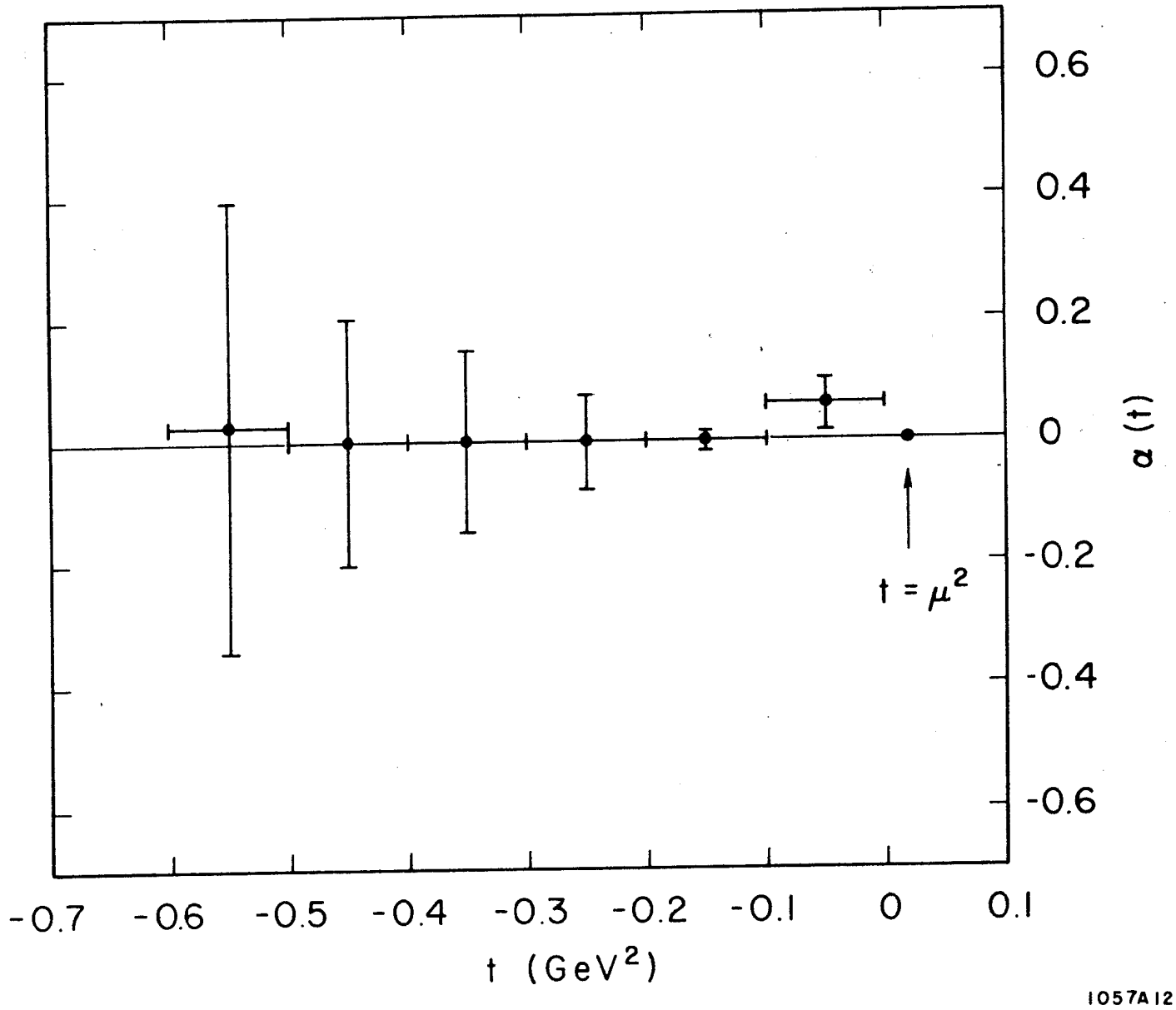

Fig. 9

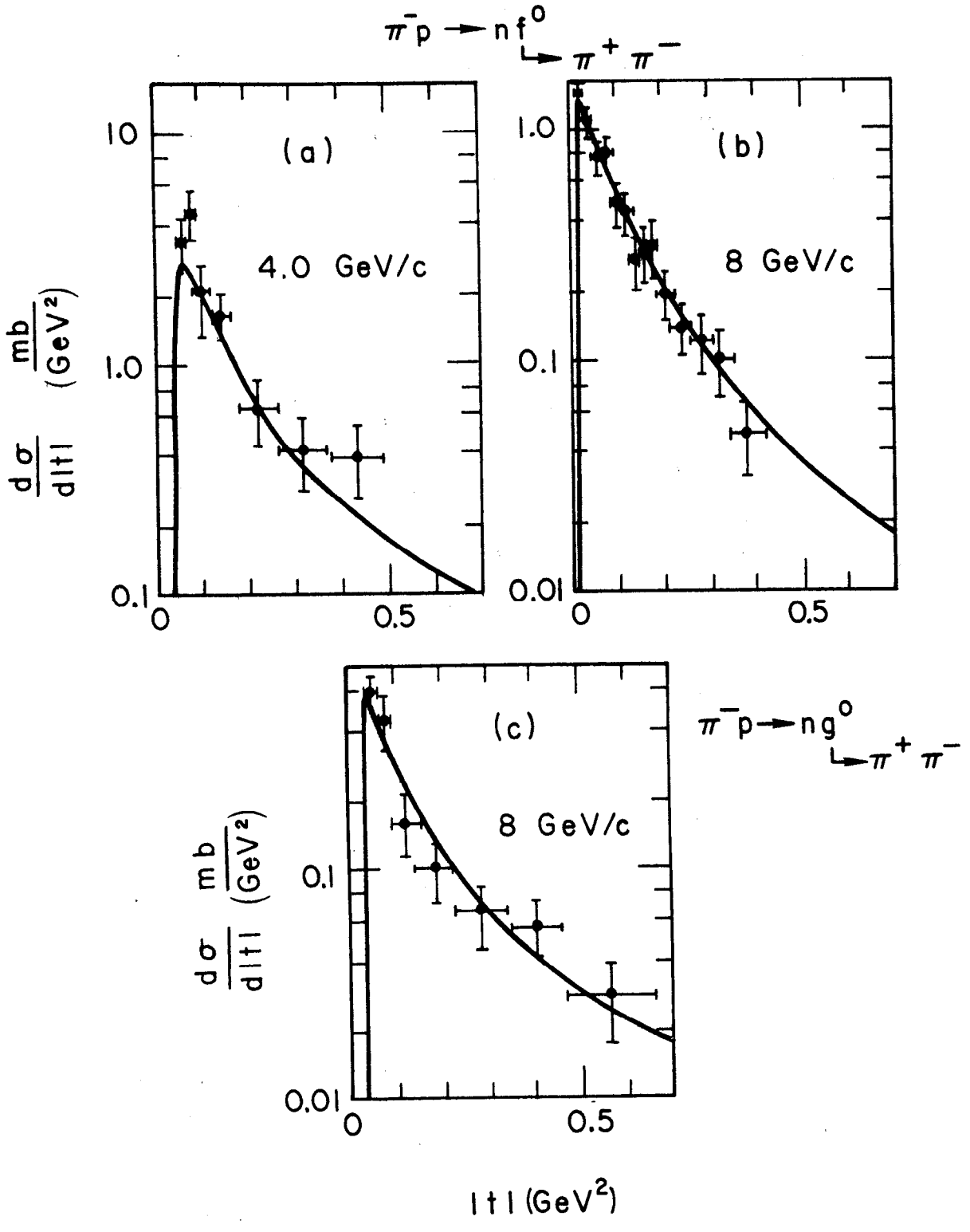
$\pi^- p \to n f^0$
$\hookrightarrow \pi^+ \pi^-$
(a)
4.0 GeV/c
(b)
8 GeV/c
(c)
8 GeV/c
$\pi^- p \to n g^0$
$\hookrightarrow \pi^+ \pi^-$
$\frac{d\sigma}{dlt1}$ $\frac{mb}{(GeV^2)}$
10
1.0
0.1
0.01
0
0.5
$|t|\ (GeV^2)$
1057B9

Fig. 10

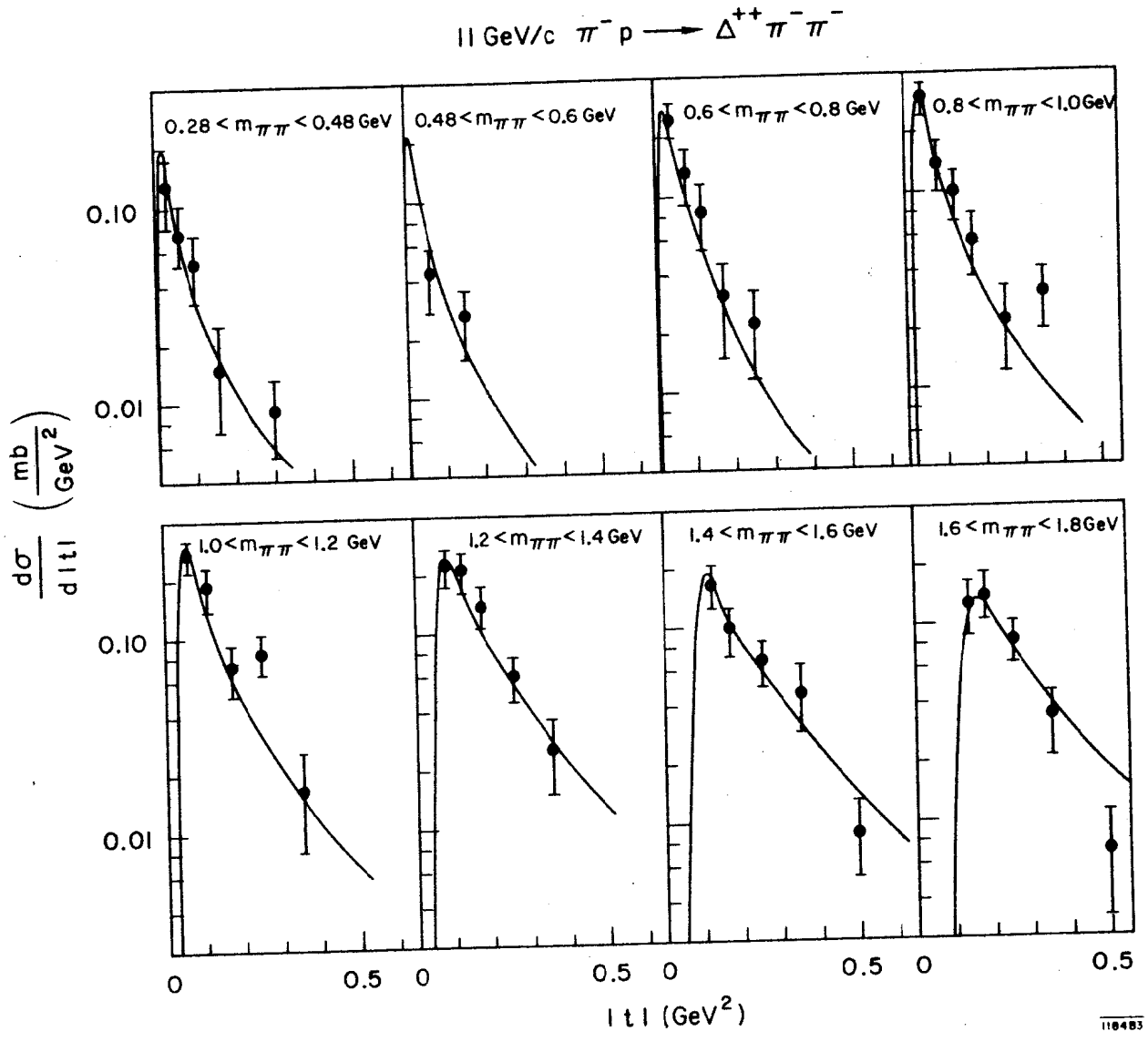
11 GeV/c $\pi^- p \longrightarrow \Delta^{++}\pi^-\pi^-$
$0.28 < m_{\pi\pi} < 0.48$ GeV
$0.48 < m_{\pi\pi} < 0.6$ GeV
$0.6 < m_{\pi\pi} < 0.8$ GeV
$0.8 < m_{\pi\pi} < 1.0$ GeV
$1.0 < m_{\pi\pi} < 1.2$ GeV
$1.2 < m_{\pi\pi} < 1.4$ GeV
$1.4 < m_{\pi\pi} < 1.6$ GeV
$1.6 < m_{\pi\pi} < 1.8$ GeV
0.10
0.01
$\frac{d\sigma}{d|t|}\left(\frac{mb}{GeV^2}\right)$
0
0.5
$|t|\ (GeV^2)$
118483

Fig. 11

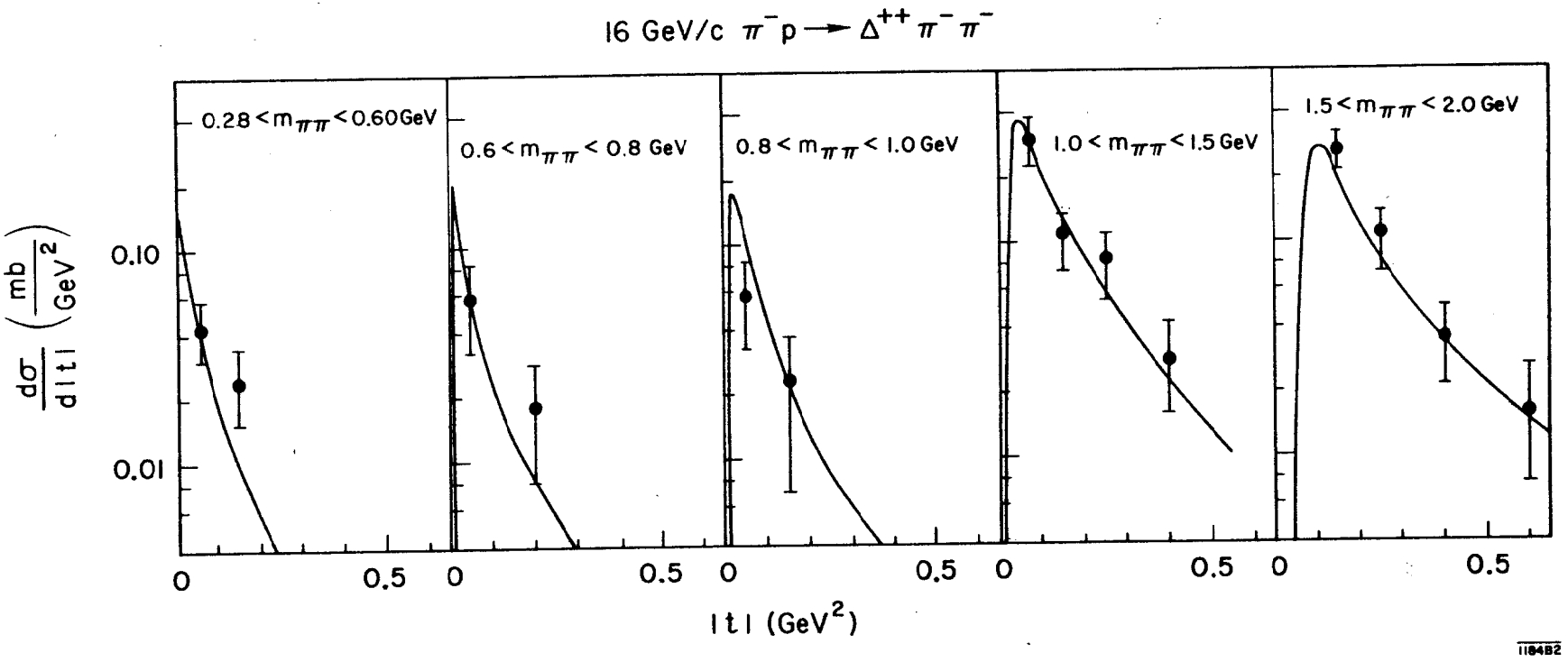
16 GeV/c $\pi^- p \rightarrow \Delta^{++} \pi^- \pi^-$
$0.28 < m_{\pi\pi} < 0.60$ GeV
$0.6 < m_{\pi\pi} < 0.8$ GeV
$0.8 < m_{\pi\pi} < 1.0$ GeV
$1.0 < m_{\pi\pi} < 1.5$ GeV
$1.5 < m_{\pi\pi} < 2.0$ GeV
$\frac{d\sigma}{dt} \left(\frac{mb}{GeV^2} \right)$
0.10
0.01
0
0.5
$|t|$ (GeV^2)
118482

Fig. 12

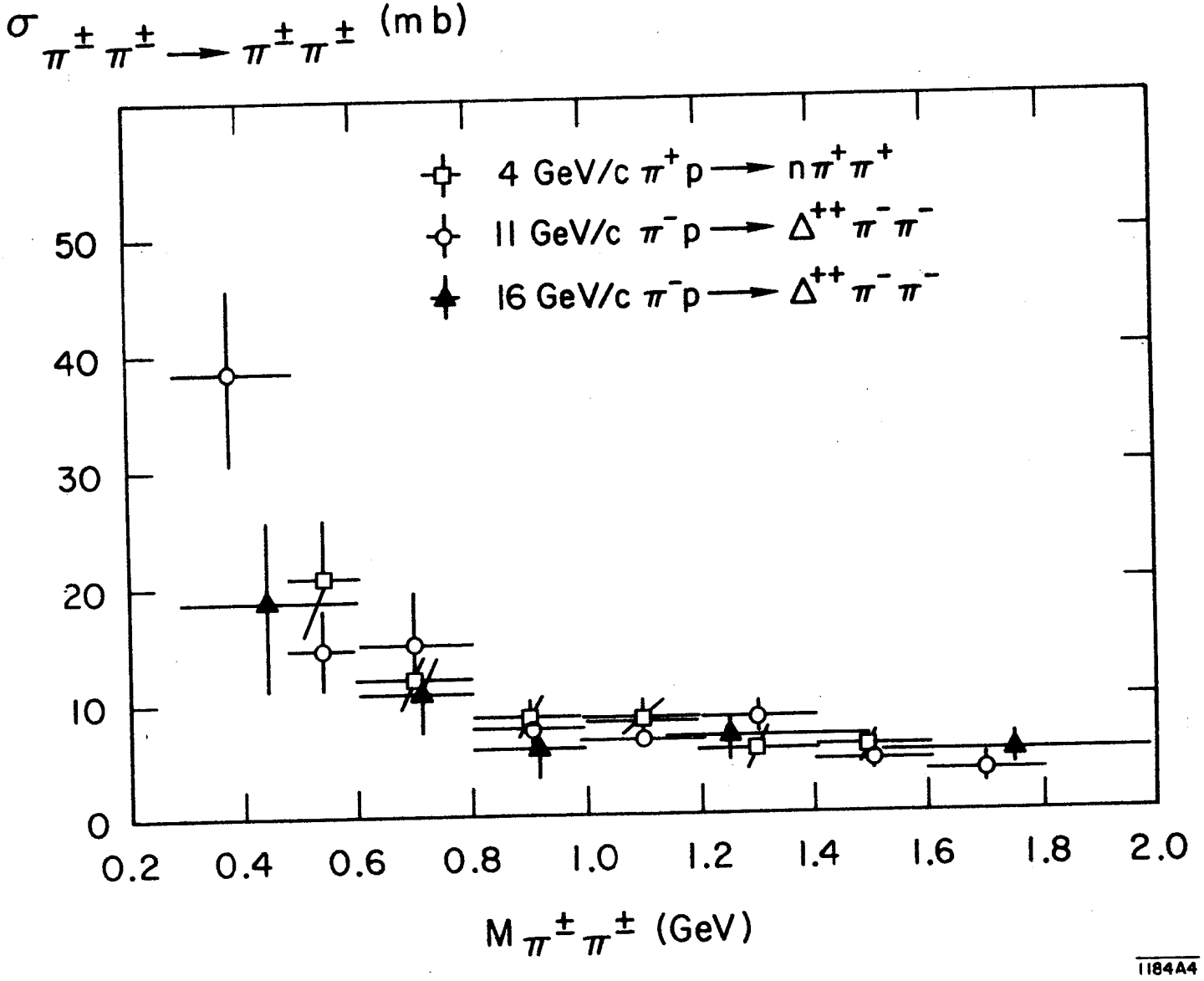
$\sigma_{\pi^\pm\pi^\pm \to \pi^\pm\pi^\pm}$ (mb)
4 GeV/c $\pi^+ p \to n\pi^+\pi^+$
11 GeV/c $\pi^- p \to \Delta^{++}\pi^-\pi^-$
16 GeV/c $\pi^- p \to \Delta^{++}\pi^-\pi^-$
50
40
30
20
10
0
0.2
0.4
0.6
0.8
1.0
1.2
1.4
1.6
1.8
2.0
$M_{\pi^\pm\pi^\pm}$ (GeV)
1184A4

Fig. 13

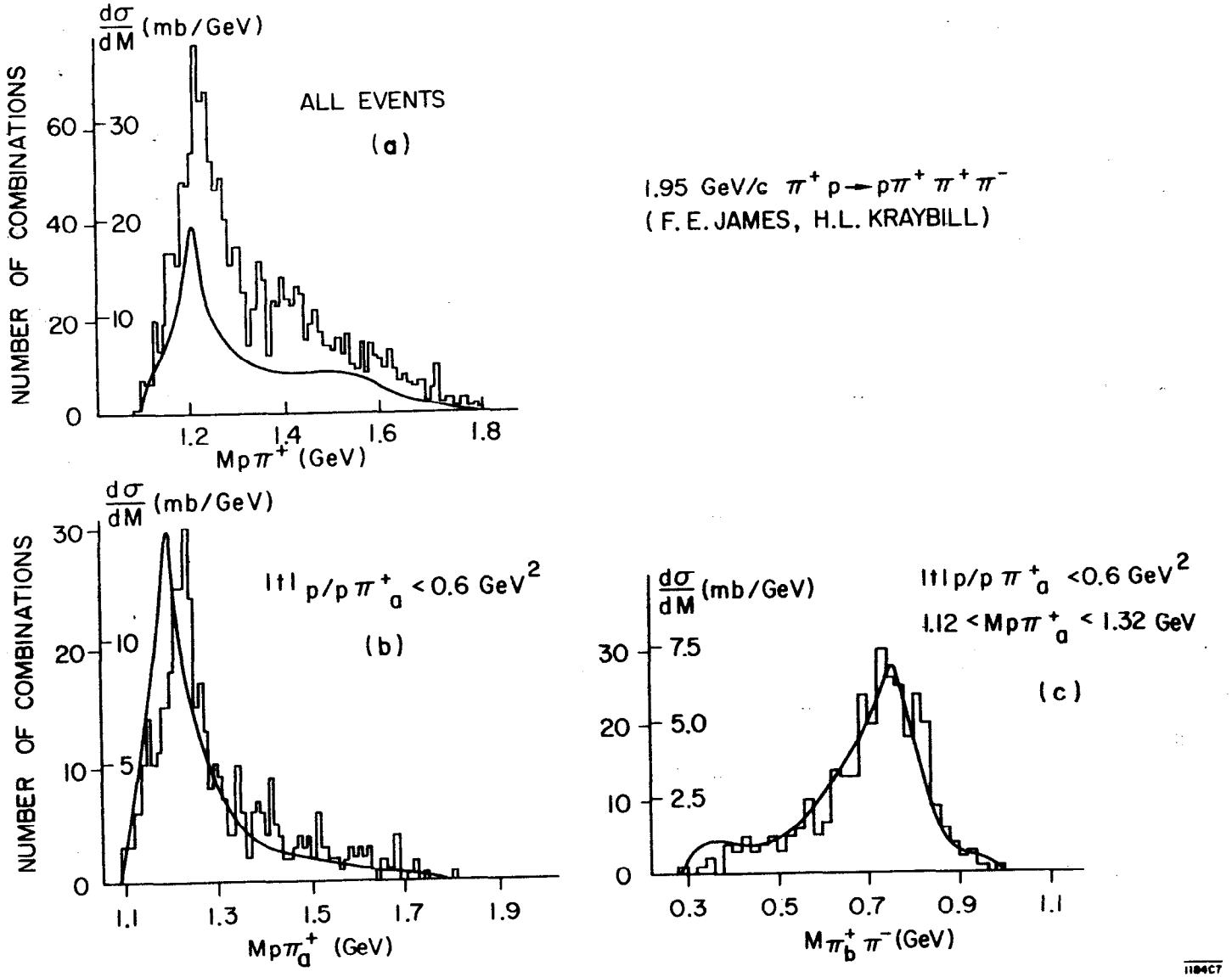
dσ/dM (mb/GeV)
ALL EVENTS
(a)
NUMBER OF COMBINATIONS
Mpπ+ (GeV)
1.95 GeV/c π+ p → pπ+ π+ π−
(F. E. JAMES, H.L. KRAYBILL)
dσ/dM (mb/GeV)
|t| p/p π+a < 0.6 GeV2
(b)
NUMBER OF COMBINATIONS
Mpπ+a (GeV)
dσ/dM (mb/GeV)
|t| p/p π+a < 0.6 GeV2
1.12 < Mpπ+a < 1.32 GeV
(c)
Mπ+b π− (GeV)
1184C7

Fig. 14

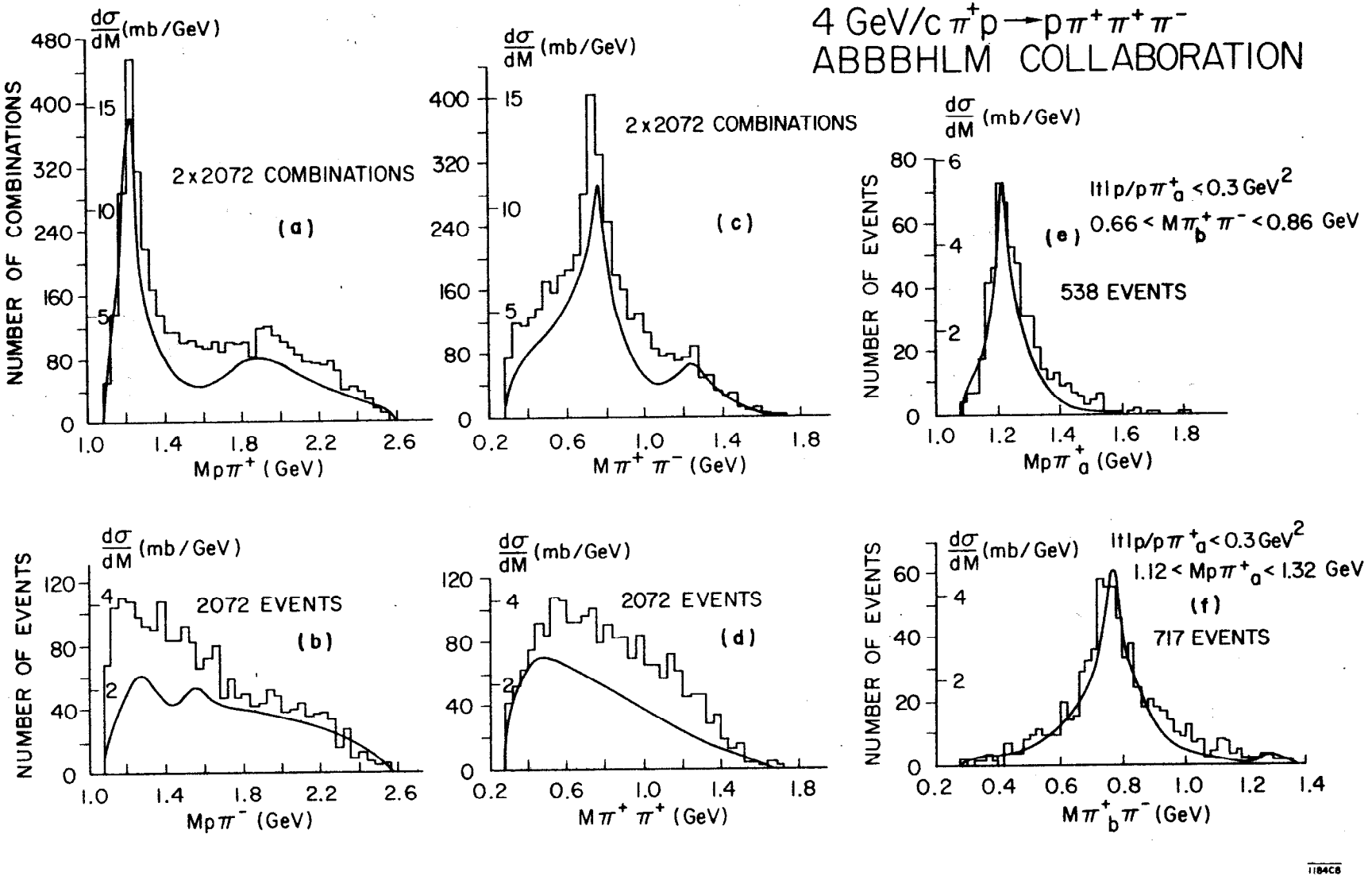
4 GeV/c $\pi^+ p \rightarrow p\pi^+\pi^+\pi^-$
ABBBHLM COLLABORATION
$\frac{d\sigma}{dM}$ (mb/GeV)
NUMBER OF COMBINATIONS
2 x 2072 COMBINATIONS
(a)
$Mp\pi^+$ (GeV)
(c)
$M\pi^+\pi^-$ (GeV)
NUMBER OF EVENTS
$|t|p/p\pi^+_a < 0.3\,GeV^2$
$0.66 < M\pi^+_b\pi^- < 0.86$ GeV
(e)
538 EVENTS
$Mp\pi^+_a$ (GeV)
2072 EVENTS
(b)
$Mp\pi^-$ (GeV)
(d)
$M\pi^+\pi^+$ (GeV)
$1.12 < Mp\pi^+_a < 1.32$ GeV
(f)
717 EVENTS
$M\pi^+_b\pi^-$ (GeV)
1184C8

Fig. 15

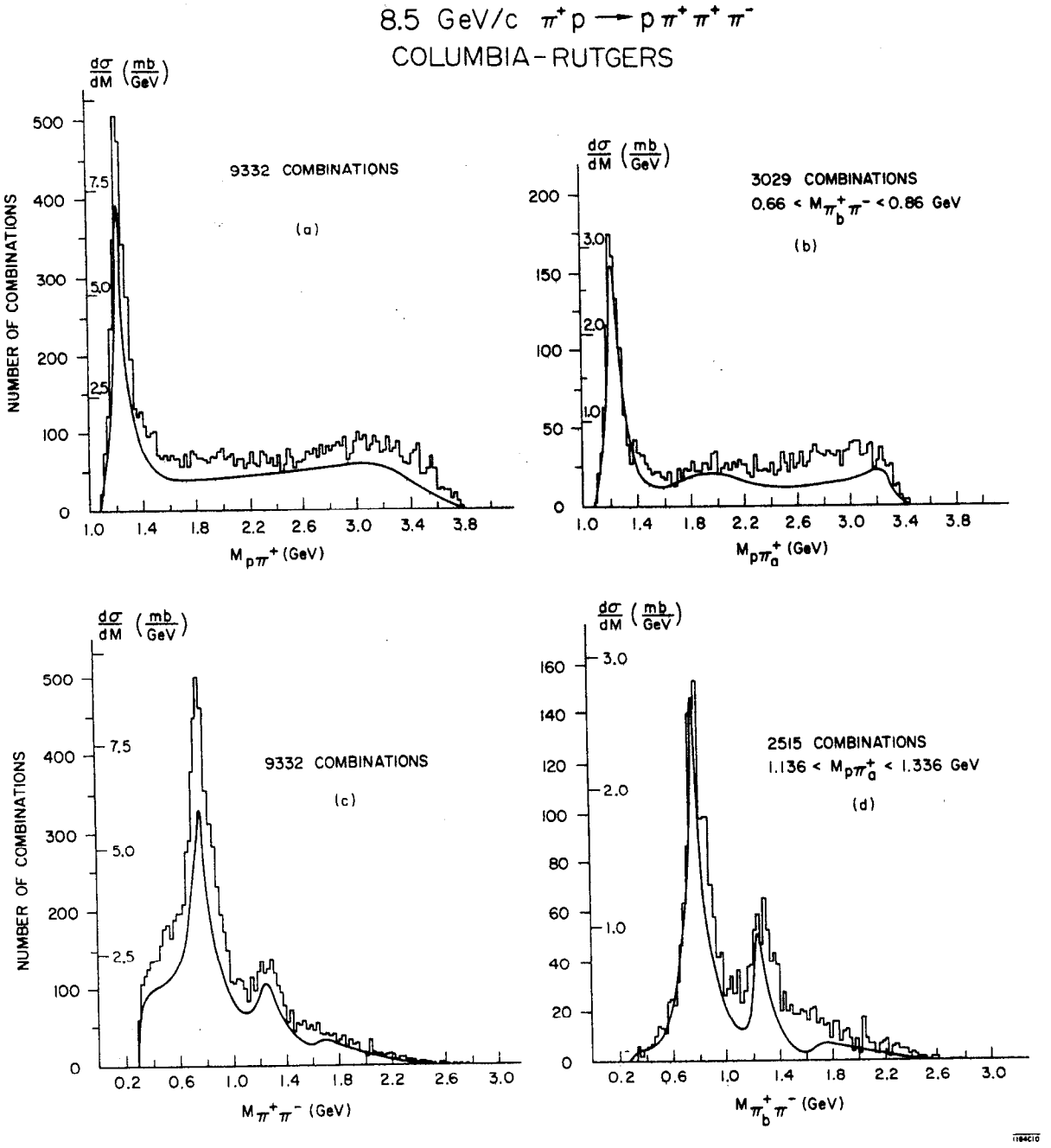
8.5 GeV/c $\pi^+ p \rightarrow p\pi^+\pi^+\pi^-$
COLUMBIA-RUTGERS
$\frac{d\sigma}{dM}$ $(\frac{mb}{GeV})$
NUMBER OF COMBINATIONS
9332 COMBINATIONS
(a)
$M_{p\pi^+}$ (GeV)
3029 COMBINATIONS
$0.66 < M_{\pi_b^+\pi^-} < 0.86$ GeV
(b)
$M_{p\pi_a^+}$ (GeV)
9332 COMBINATIONS
(c)
$M_{\pi^+\pi^-}$ (GeV)
2515 COMBINATIONS
$1.136 < M_{p\pi_a^+} < 1.336$ GeV
(d)
$M_{\pi_b^+\pi^-}$ (GeV)

Fig. 16

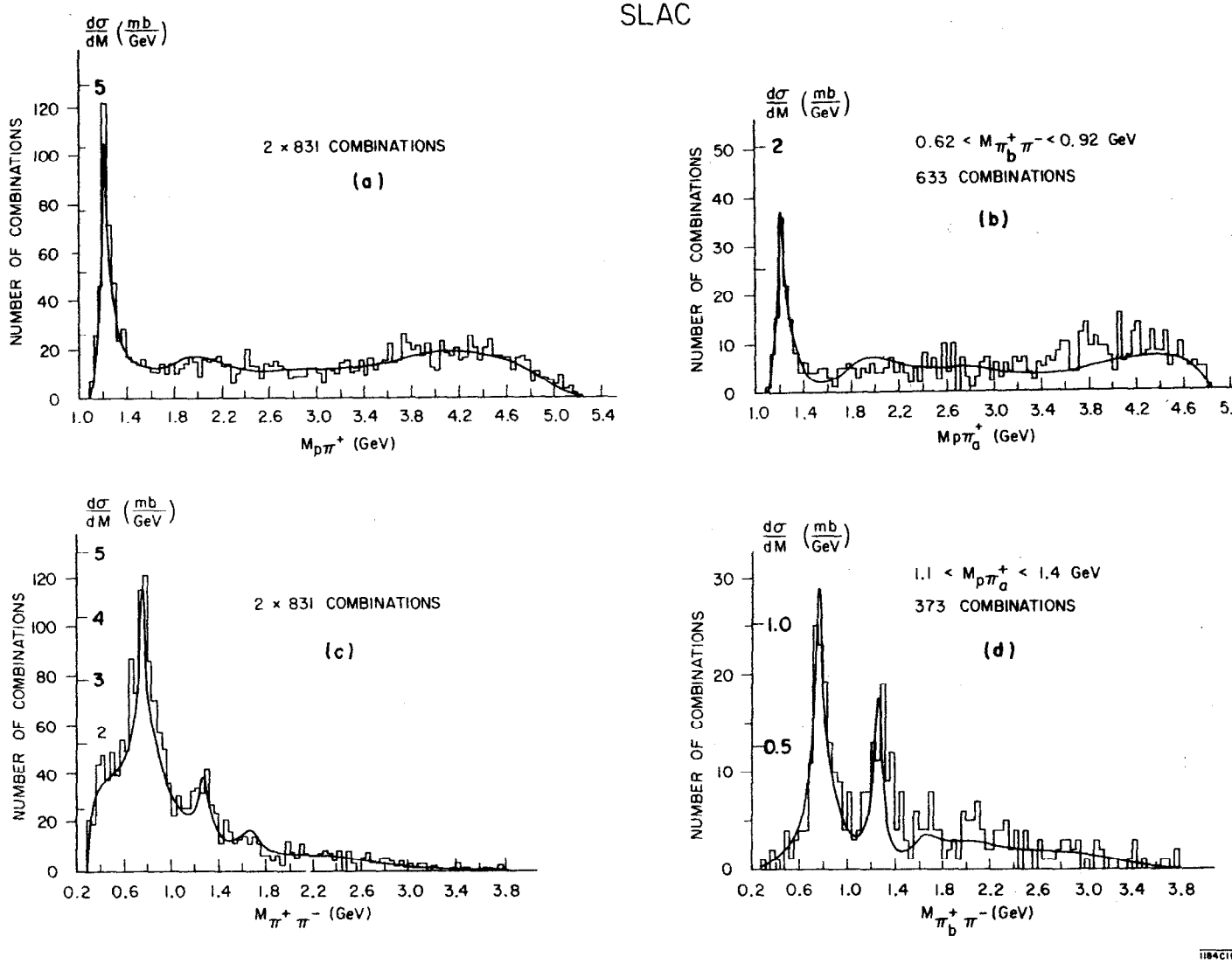
16 GeV/c $\pi^+ p \rightarrow p\pi^+\pi^+\pi^-$
SLAC
$\frac{d\sigma}{dM}$ $(\frac{mb}{GeV})$
NUMBER OF COMBINATIONS
2 × 831 COMBINATIONS
(a)
$M_{p\pi^+}$ (GeV)
$0.62 < M_{\pi_b^+\pi^-} < 0.92$ GeV
633 COMBINATIONS
(b)
$Mp\pi_a^+$ (GeV)
2 × 831 COMBINATIONS
(c)
$M_{\pi^+\pi^-}$ (GeV)
$1.1 < M_{p\pi_a^+} < 1.4$ GeV
373 COMBINATIONS
(d)
$M_{\pi_b^+\pi^-}$ (GeV)
1184C11

Fig. 17

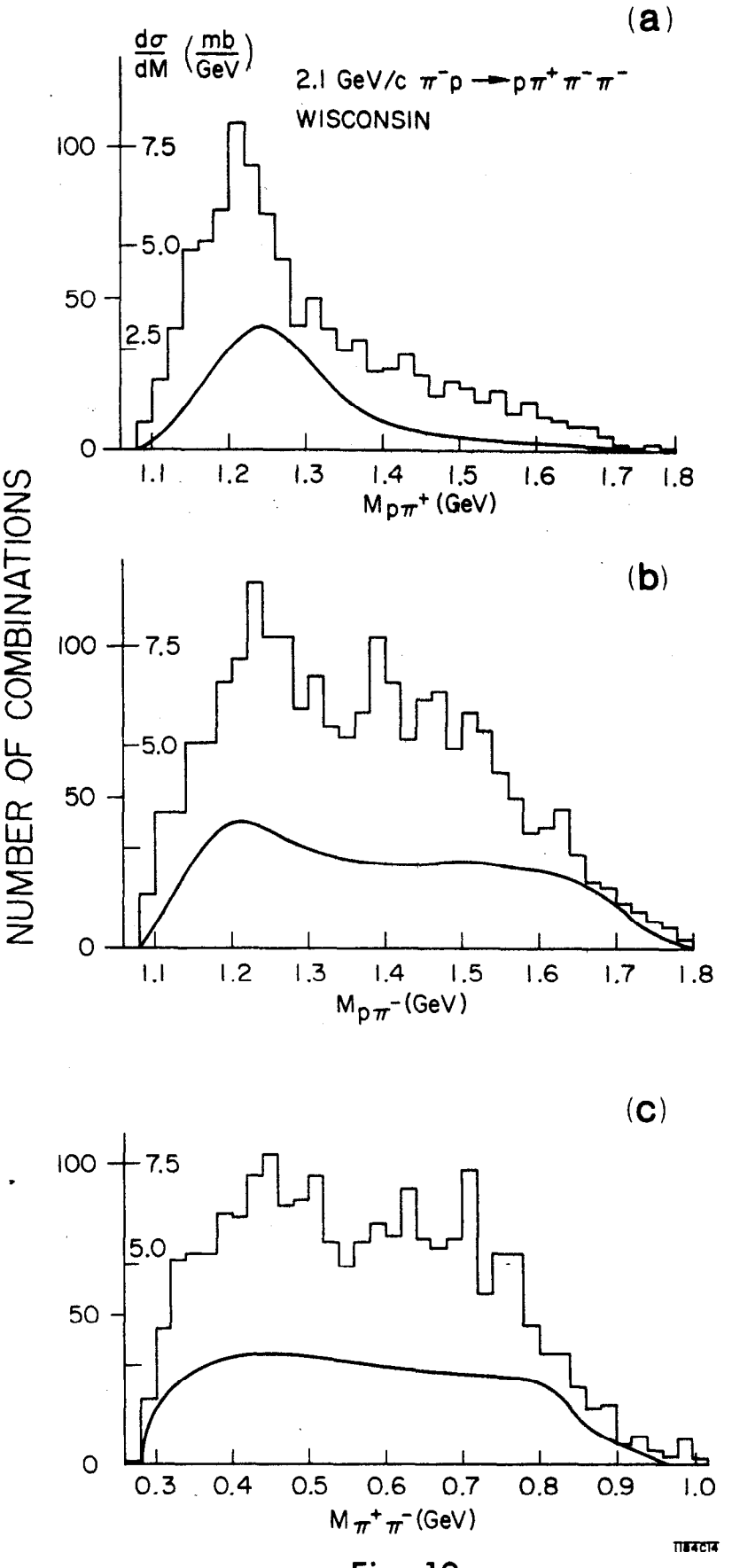
(a)
dσ/dM (mb/GeV)
2.1 GeV/c π⁻p → pπ⁺π⁻π⁻
WISCONSIN
100
7.5
5.0
50
2.5
0
1.1 1.2 1.3 1.4 1.5 1.6 1.7 1.8
Mpπ⁺ (GeV)
(b)
NUMBER OF COMBINATIONS
100
7.5
5.0
50
0
1.1 1.2 1.3 1.4 1.5 1.6 1.7 1.8
Mpπ⁻ (GeV)
(c)
100
7.5
5.0
50
0
0.3 0.4 0.5 0.6 0.7 0.8 0.9 1.0
Mπ⁺π⁻ (GeV)
1184C14

Fig. 18

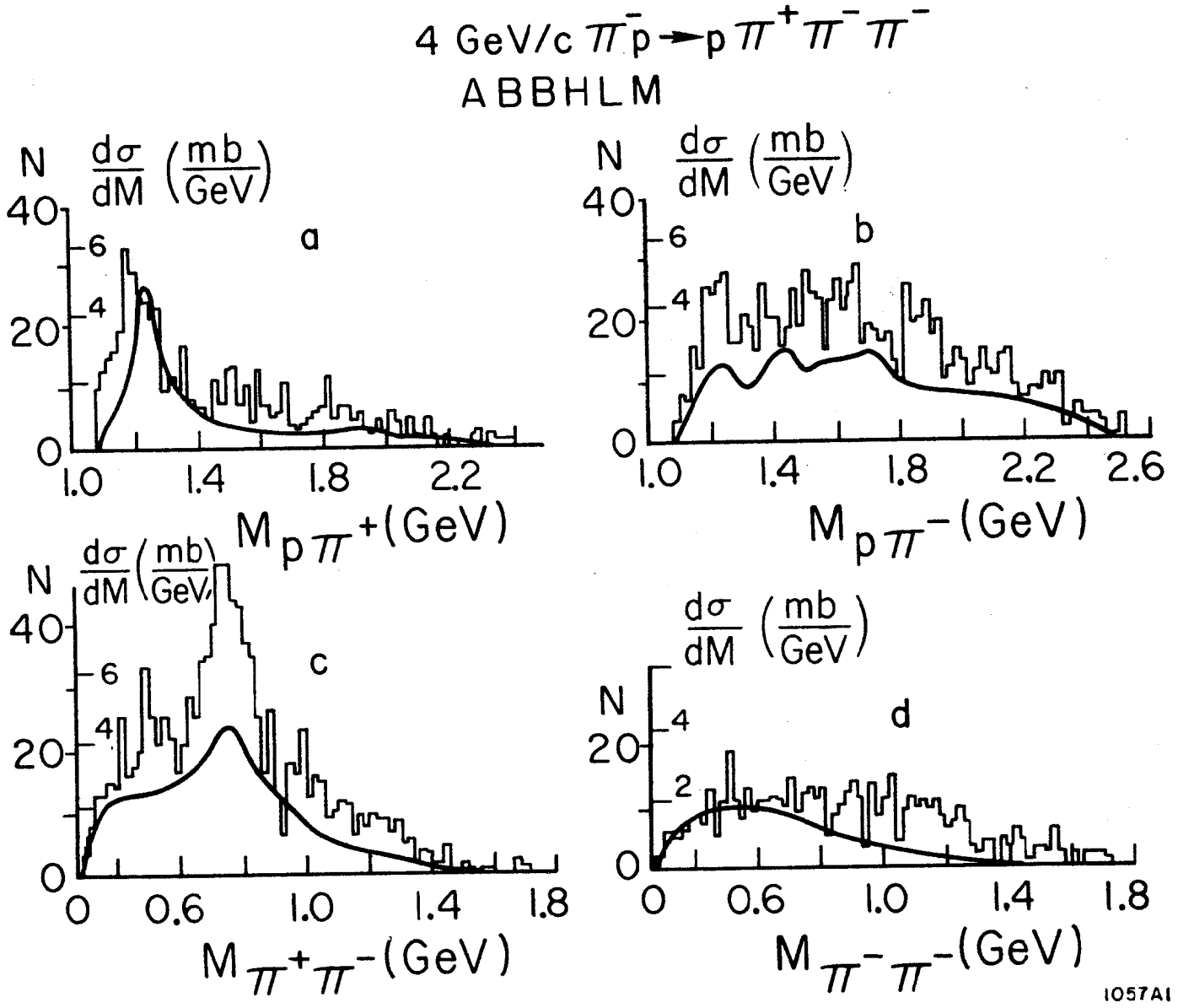
4 GeV/c $\pi^- p \to p\pi^+\pi^-\pi^-$
A B B H L M
N
$\frac{d\sigma}{dM}\left(\frac{mb}{GeV}\right)$
a
b
c
d
$M_{p\pi^+}$(GeV)
$M_{p\pi^-}$(GeV)
$M_{\pi^+\pi^-}$(GeV)
$M_{\pi^-\pi^-}$(GeV)
1057A1

Fig. 19

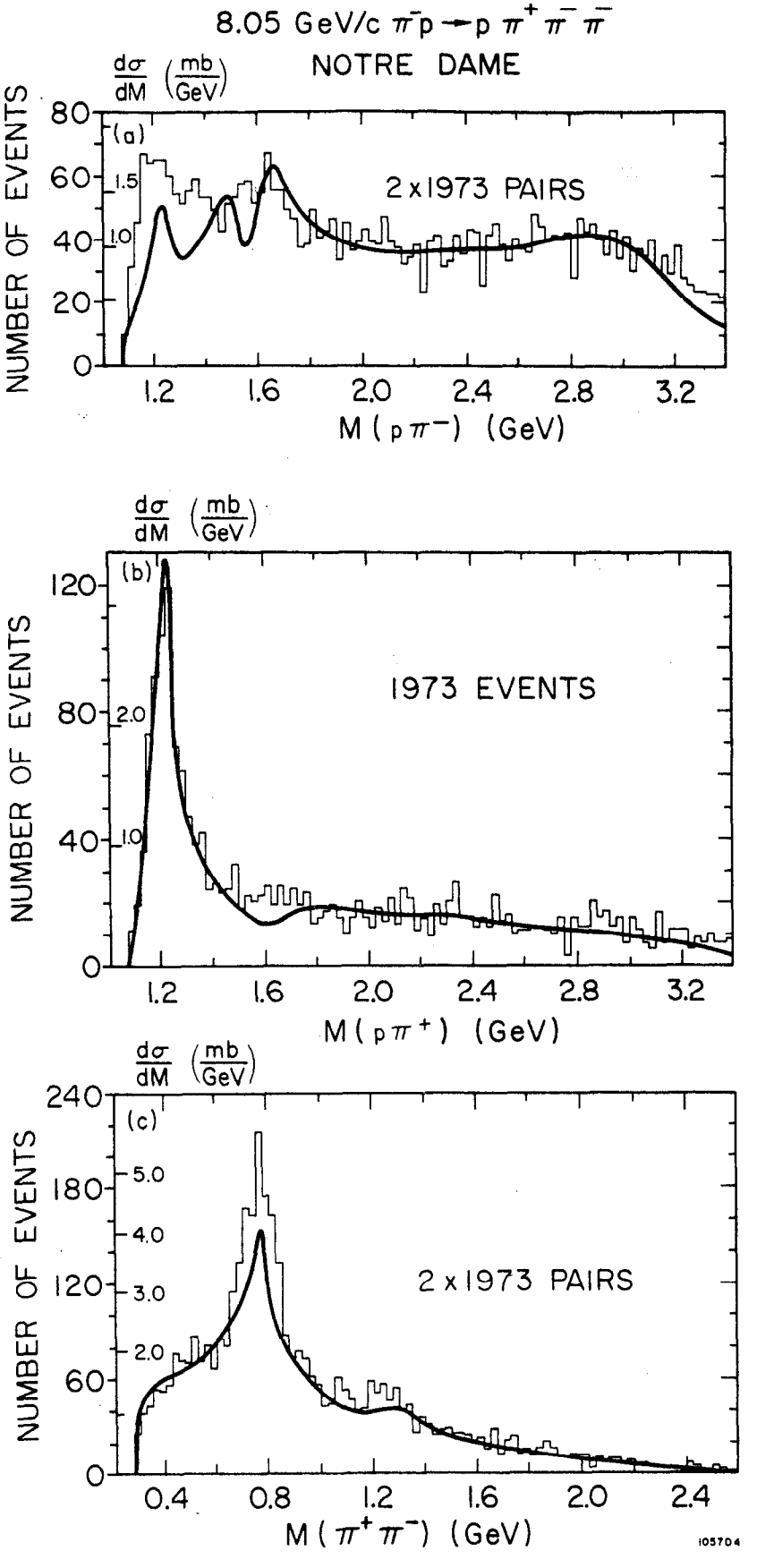
8.05 GeV/c $\pi^- p \to p\,\pi^+\pi^-\pi^-$
NOTRE DAME
$\frac{d\sigma}{dM}$ $\left(\frac{mb}{GeV}\right)$
NUMBER OF EVENTS
(a)
2 x 1973 PAIRS
$M(p\pi^-)$ (GeV)
(b)
1973 EVENTS
$M(p\pi^+)$ (GeV)
(c)
2 x 1973 PAIRS
$M(\pi^+\pi^-)$ (GeV)
105704

Fig. 20

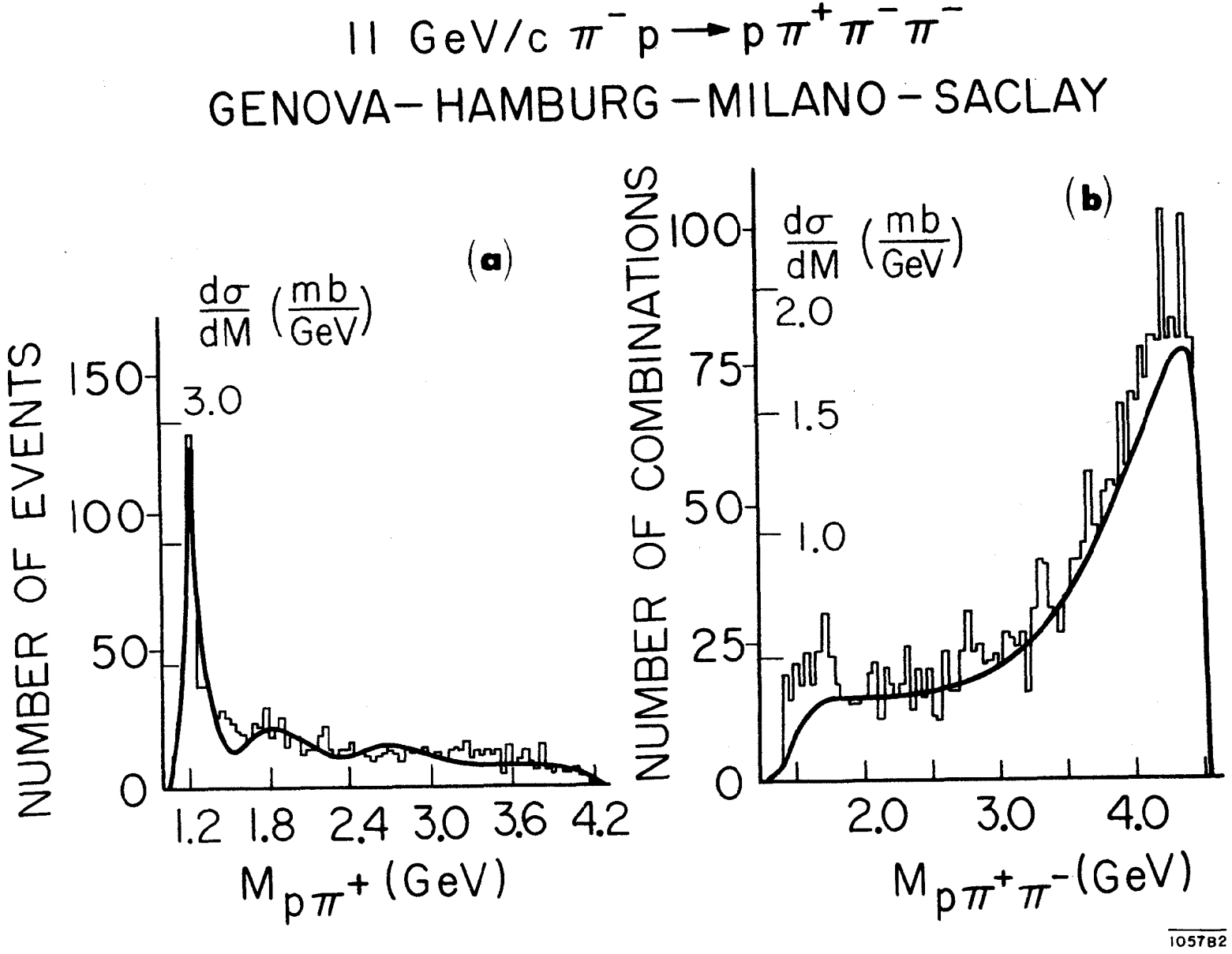
11 GeV/c $\pi^- p \rightarrow p\pi^+\pi^-\pi^-$
GENOVA – HAMBURG – MILANO – SACLAY
(a)
$\frac{d\sigma}{dM}$ $(\frac{mb}{GeV})$
NUMBER OF EVENTS
150
100
50
0
3.0
1.2 1.8 2.4 3.0 3.6 4.2
$M_{p\pi^+}$ (GeV)
(b)
$\frac{d\sigma}{dM}$ $(\frac{mb}{GeV})$
NUMBER OF COMBINATIONS
100
75
50
25
0
2.0
1.5
1.0
2.0 3.0 4.0
$M_{p\pi^+\pi^-}$ (GeV)
105782

Fig. 21

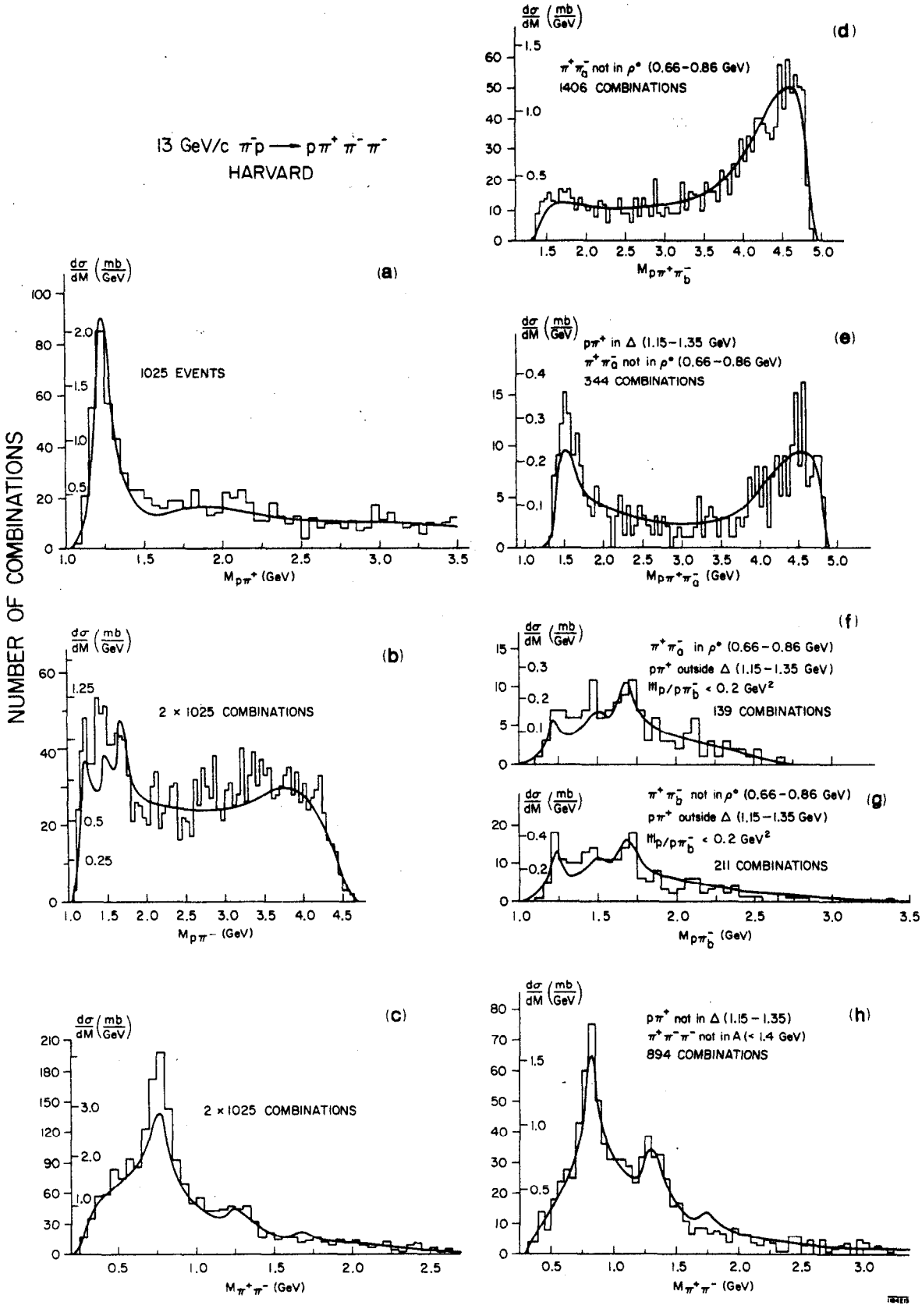
13 GeV/c $\pi^- p \longrightarrow p\pi^+\pi^-\pi^-$
HARVARD
NUMBER OF COMBINATIONS
(a)
1025 EVENTS
$M_{p\pi^+}$ (GeV)
(b)
2 × 1025 COMBINATIONS
$M_{p\pi^-}$ (GeV)
(c)
2 × 1025 COMBINATIONS
$M_{\pi^+\pi^-}$ (GeV)
(d)
$\pi^+\pi_a^-$ not in ρ^0 (0.66–0.86 GeV)
1406 COMBINATIONS
$M_{p\pi^+\pi_b^-}$
(e)
$p\pi^+$ in Δ (1.15–1.35 GeV)
$\pi^+\pi_a^-$ not in ρ^0 (0.66–0.86 GeV)
344 COMBINATIONS
$M_{p\pi^+\pi_a^-}$ (GeV)
(f)
$\pi^+\pi_a^-$ in ρ^0 (0.66–0.86 GeV)
$p\pi^+$ outside Δ (1.15–1.35 GeV)
$|t|_{p/p\pi_b^-}$ < 0.2 GeV^2
139 COMBINATIONS
(g)
$\pi^+\pi_b^-$ not in ρ^0 (0.66–0.86 GeV)
$p\pi^+$ outside Δ (1.15–1.35 GeV)
$|t|_{p/p\pi_b^-}$ < 0.2 GeV^2
211 COMBINATIONS
$M_{p\pi_b^-}$ (GeV)
(h)
$p\pi^+$ not in Δ (1.15–1.35)
$\pi^+\pi^-\pi^-$ not in A (< 1.4 GeV)
894 COMBINATIONS
$M_{\pi^+\pi^-}$ (GeV)

Fig. 22

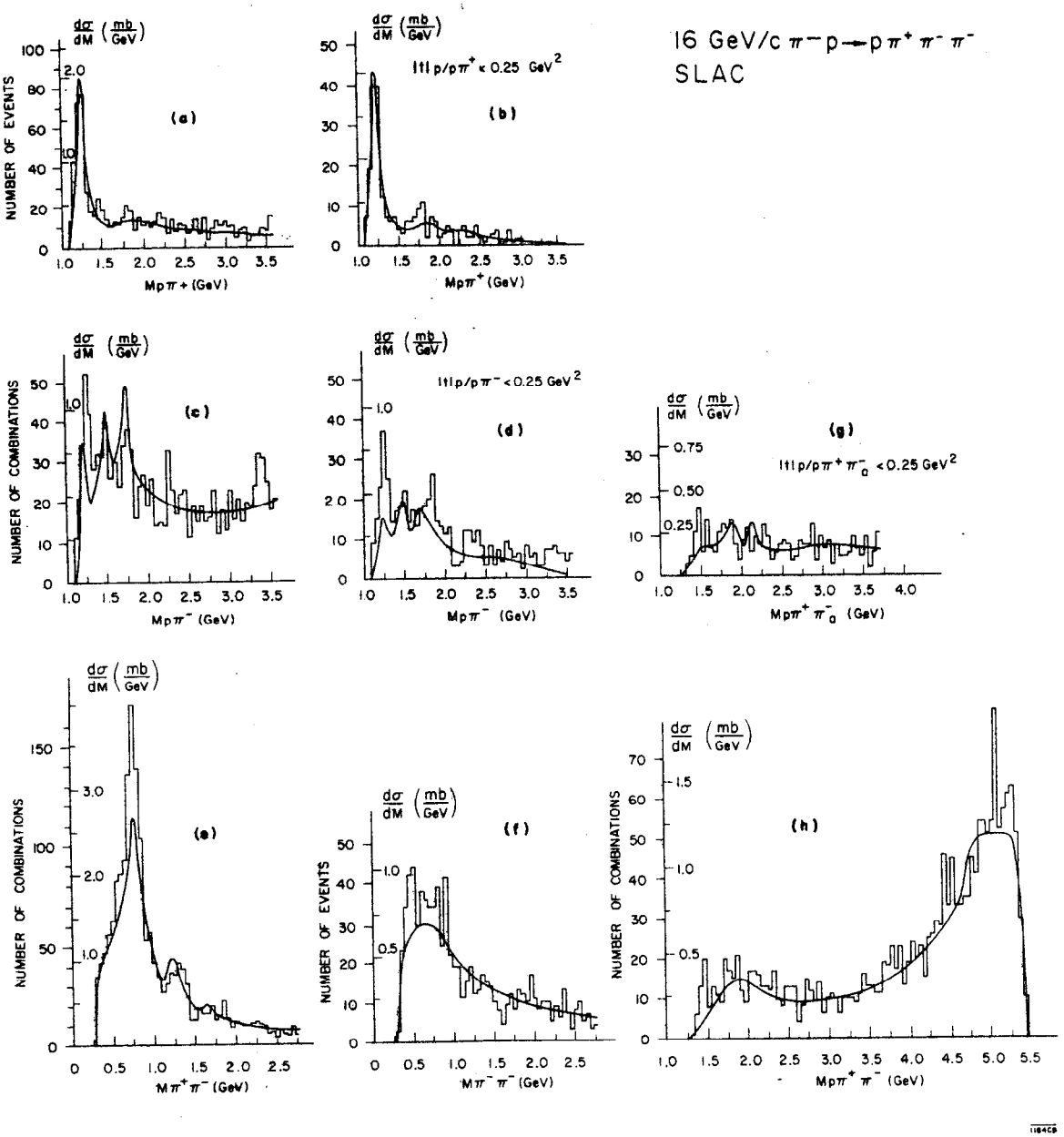
16 GeV/c π⁻p → pπ⁺π⁻π⁻
SLAC
dσ/dM (mb/GeV)
NUMBER OF EVENTS
(a)
Mpπ⁺ (GeV)
(b)
|t|p/pπ⁺ < 0.25 GeV²
Mpπ⁺ (GeV)
NUMBER OF COMBINATIONS
(c)
Mpπ⁻ (GeV)
(d)
|t|p/pπ⁻ < 0.25 GeV²
Mpπ⁻ (GeV)
(g)
|t|p/pπ⁺π⁻₀ < 0.25 GeV²
Mpπ⁺π⁻₀ (GeV)
(e)
Mπ⁺π⁻ (GeV)
(f)
Mπ⁻π⁻ (GeV)
(h)
Mpπ⁺π⁻ (GeV)

Fig. 23

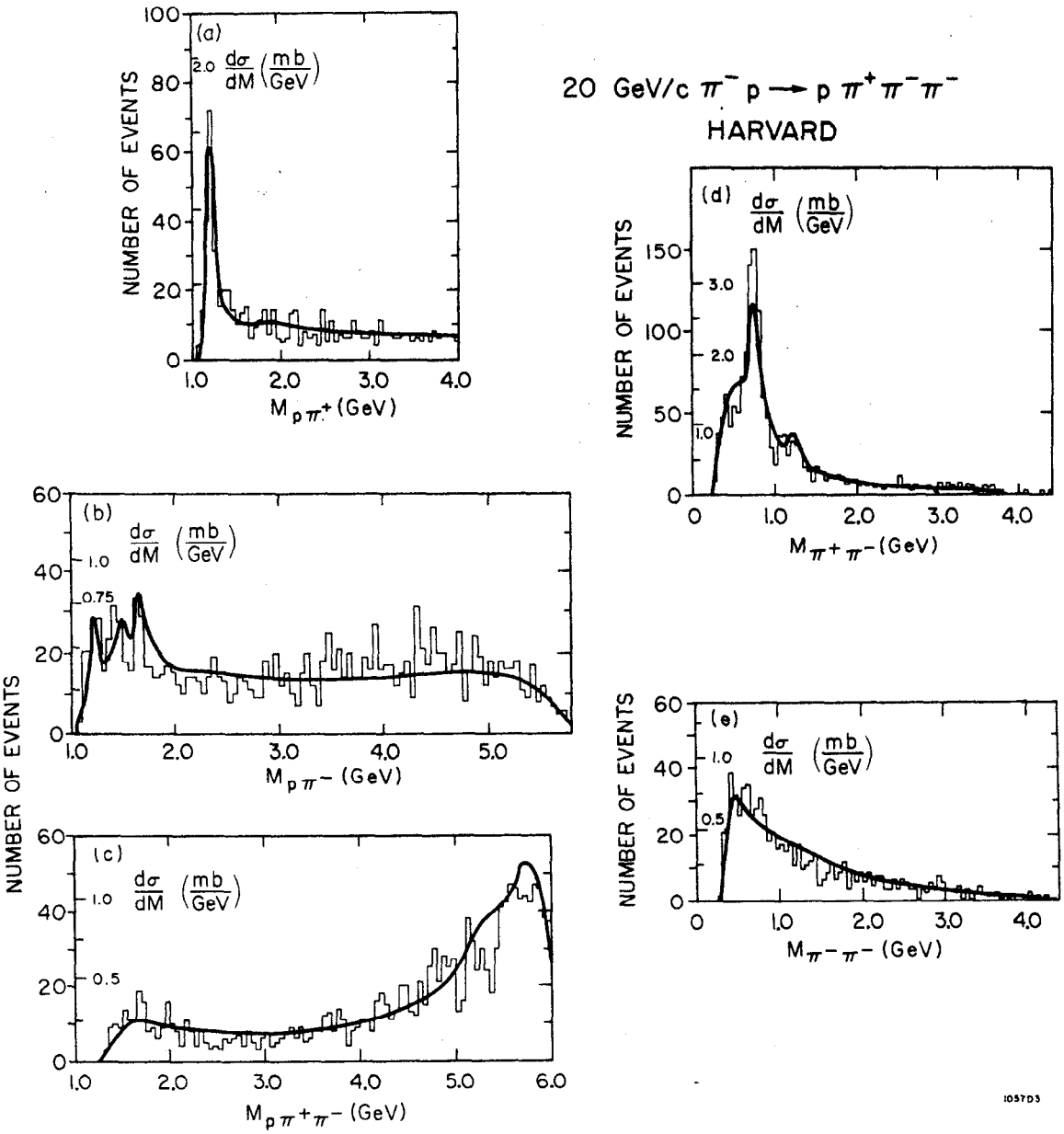
20 GeV/c $\pi^- p \rightarrow p \pi^+ \pi^- \pi^-$
HARVARD
(a)
$\frac{d\sigma}{dM}\left(\frac{mb}{GeV}\right)$
NUMBER OF EVENTS
$M_{p\pi^+}$ (GeV)
(b)
$M_{p\pi^-}$ (GeV)
(c)
$M_{p\pi^+\pi^-}$ (GeV)
(d)
$M_{\pi^+\pi^-}$ (GeV)
(e)
$M_{\pi^-\pi^-}$ (GeV)
1057D3

Fig. 24

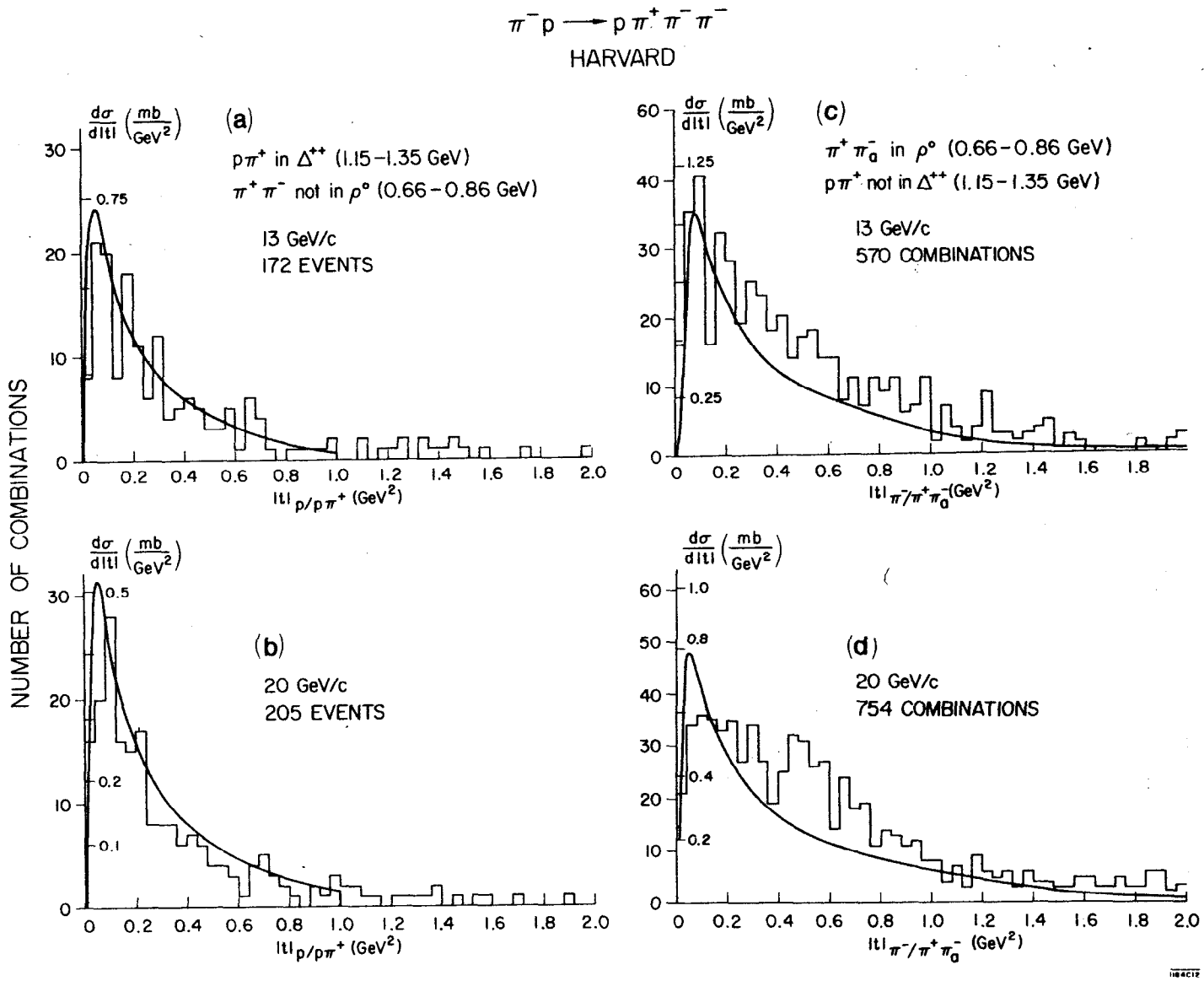
$\pi^- p \longrightarrow p\pi^+\pi^-\pi^-$
HARVARD
NUMBER OF COMBINATIONS
(a)
$p\pi^+$ in Δ^{++} (1.15–1.35 GeV)
$\pi^+\pi^-$ not in ρ^0 (0.66–0.86 GeV)
13 GeV/c
172 EVENTS
(b)
20 GeV/c
205 EVENTS
(c)
$\pi^+\pi^-_a$ in ρ^0 (0.66–0.86 GeV)
$p\pi^+$ not in Δ^{++} (1.15–1.35 GeV)
13 GeV/c
570 COMBINATIONS
(d)
20 GeV/c
754 COMBINATIONS
$\frac{d\sigma}{dltl}\left(\frac{mb}{GeV^2}\right)$
$ltl_{p/p\pi^+}$ (GeV^2)
$ltl_{\pi^-/\pi^+\pi^-_a}$ (GeV^2)

Fig. 25

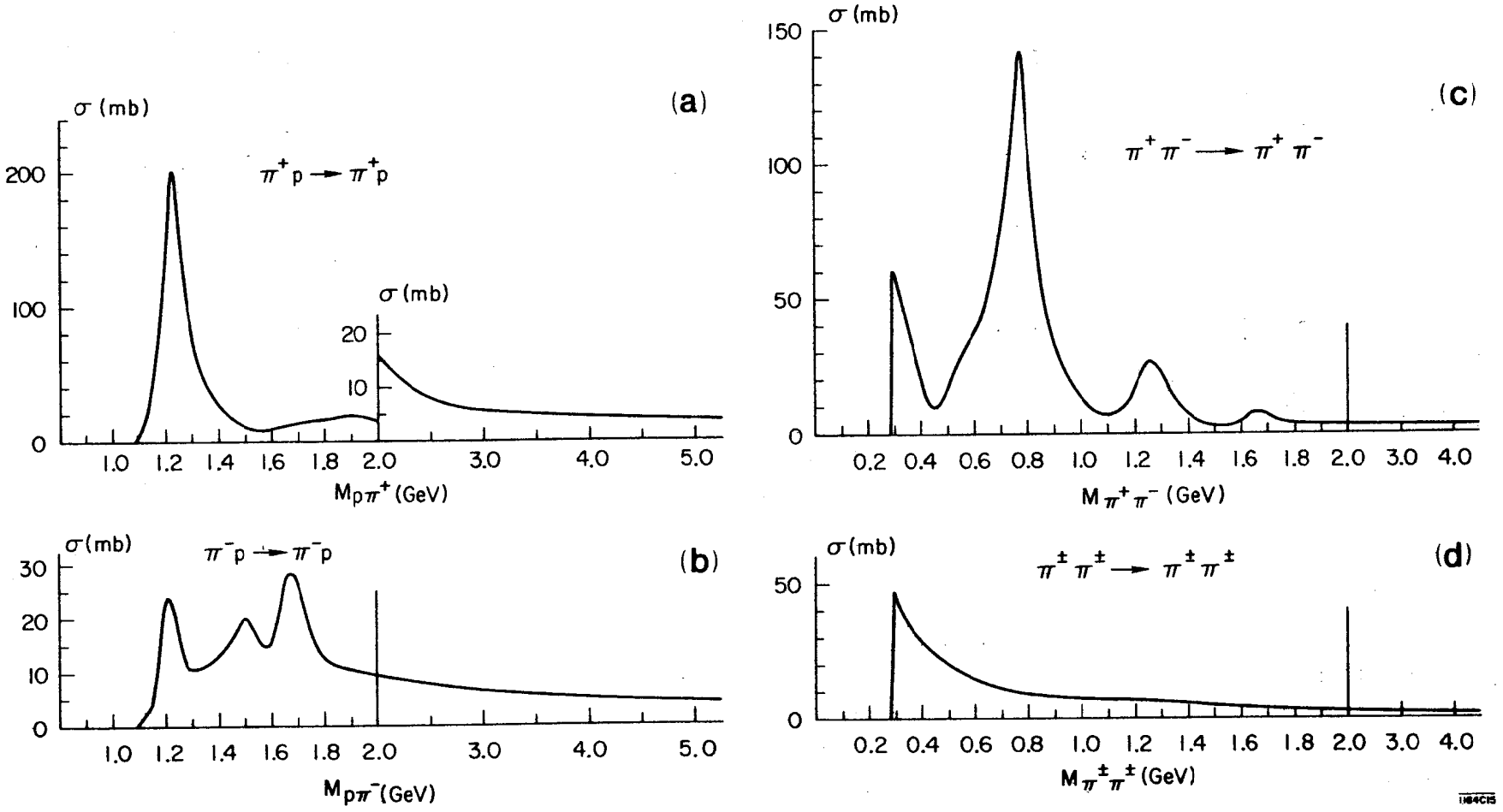
σ (mb)
(a)
$\pi^+ p \rightarrow \pi^+ p$
200
100
0
σ (mb)
20
10
1.0 1.2 1.4 1.6 1.8 2.0 3.0 4.0 5.0
$M_{p\pi^+}$ (GeV)
σ (mb)
(b)
$\pi^- p \rightarrow \pi^- p$
30
20
10
0
1.0 1.2 1.4 1.6 1.8 2.0 3.0 4.0 5.0
$M_{p\pi^-}$ (GeV)
σ (mb)
(c)
$\pi^+ \pi^- \rightarrow \pi^+ \pi^-$
150
100
50
0
0.2 0.4 0.6 0.8 1.0 1.2 1.4 1.6 1.8 2.0 3.0 4.0
$M_{\pi^+\pi^-}$ (GeV)
σ (mb)
(d)
$\pi^\pm \pi^\pm \rightarrow \pi^\pm \pi^\pm$
50
0
0.2 0.4 0.6 0.8 1.0 1.2 1.4 1.6 1.8 2.0 3.0 4.0
$M_{\pi^\pm\pi^\pm}$ (GeV)
1164C15

Fig. 26